# Genetic and pharmacological reduction of CDK14 mitigates synucleinopathy

**Authors:** Jean-Louis A. Parmasad[1,2,†], Konrad M. Ricke[1,2,3†], Morgan G. Stykel[4], Brodie Buchner-Duby[4], Eric Lian[5,6], Benjamin Nguyen[1,2,3], Nathalie A. Lengacher[1,3,5], Haley M. Geertsma[1,2,3], Amanda Bruce[1,2], Steve M. Callaghan[1,2,3], Alvin Joselin[7], Julianna J. Tomlinson[1,3,5], Michael G. Schlossmacher[1,3,5], William L. Stanford[2,5,6], Patrik Brundin[8], Scott D. Ryan[4], and Maxime W.C. Rousseaux[1,2,3,6,*]

**Affiliations:**

[1] University of Ottawa Brain and Mind Research Institute, Ottawa, ON

[2] Department of Cellular and Molecular Medicine, University of Ottawa, Ottawa, ON

[3] Aligning Science Across Parkinson's (ASAP) Collaborative Research Network, Chevy Chase, MD

[4] Department of Molecular and Cellular Biology, University of Guelph, Guelph, ON

[5] Program in Neuroscience, Ottawa Hospital Research Institute, Ottawa, ON

[6] Ottawa Institute for Systems Biology, University of Ottawa, Ottawa, ON

[7] Hotchkiss Brain Institute, Department of Clinical Neurosciences, University of Calgary, Calgary, AB

[8] Parkinson's Disease Center, Department of Neurodegenerative Science, Van Andel Institute, Grand Rapids, MI

[†]Authors contributed equally

*Corresponding author. Email: max.rousseaux@uottawa.ca

28 **One Sentence Summary:**

29 Loss of CDK14 mitigates α-Synuclein pathology in Parkinson's disease (PD) mouse models and
30 in human neurons, highlighting CDK14 as a druggable target for the treatment of PD.

31

32 **Abstract:**

33 Parkinson's disease (PD) is a debilitating neurodegenerative disease characterized by the loss of
34 midbrain dopaminergic neurons (DaNs) and the abnormal accumulation of α-Synuclein (α-Syn)
35 protein. Currently, no treatment can slow nor halt neurodegeneration. Multiplications and
36 mutations of the α-Syn gene (*SNCA*) cause PD-associated syndromes and animal models that
37 overexpress α-Syn replicate several features of PD. Decreasing total α-Syn levels, therefore, is an
38 attractive approach to slow down neurodegeneration in patients with a 'synucleinopathy'. We
39 previously performed a genetic screen for modifiers of α-Syn levels, and found CDK14, a kinase
40 of largely unknown function as a regulator of α-Syn. To test the potential therapeutic effects of
41 CDK14 reduction in PD, we decreased Cdk14 in two mouse models of synucleinopathy. We found
42 that reduction of Cdk14 mitigated neuropathological and neurobehavioral sequelae associated with
43 α-Syn overexpression. We further validated these findings in PD patient neurons. Finally, we
44 leveraged the recent discovery of a covalent inhibitor of CDK14 to determine whether this target
45 is pharmacologically tractable *ex vivo*. We found that in both mouse and human neurons, CDK14
46 inhibition decreases total and pathologically aggregated α-Syn. In summary, we suggest that
47 CDK14 represents a novel therapeutic target for PD-associated synucleinopathy.

48

## INTRODUCTION

Parkinson's disease (PD) is a neurodegenerative disease that affects over 10 million individuals worldwide (*1*,*2*). Individuals with PD present with motor symptoms such as bradykinesia, rigidity, shuffling gait, and resting tremor, as well as non-motor symptoms such as constipation, anosmia and sleep disturbances (*3–5*). Neuropathologically, typical PD is characterized by the loss of dopaminergic neurons (DaNs) in the substantia nigra pars compacta (SN) as well as the accumulation of α-synuclein (α-Syn) containing inclusions termed Lewy bodies and Lewy neurites (collectively: Lewy pathology) in surviving neurons (*6–8*). Current treatments address motor deficits, but are less effective on non-motor aspects of the disease and cannot slow down nor halt neurodegeneration in PD (*9*). Therefore, identifying new druggable targets for PD is clearly warranted. In addition to being abundantly present in Lewy pathology, point mutations and multiplications in the gene encoding α-Syn, *SNCA*, underlie monogenic variants of PD (*10*,*11*). Increased levels of *SNCA* mRNA are also observed in laser captured SN DaNs from PD patients (*12*), and animal models that overexpress α-Syn replicate several features of PD (*13–15*). Thus, there is a clear link between increased α-Syn dosage and PD pathogenesis, highlighting a crucial role of α-Syn in the manifestation of PD (*16–19*).

Since α-Syn dosage is linked to PD, decreasing total α-Syn levels may be a feasible approach to mitigate neurodegeneration in PD patients, regardless of whether oligomeric or fibrillar α-Syn is the toxic culprit. *Snca*-knockout (KO) mice are viable and fertile but display mild cognitive impairments, suggesting that a modest amount of cerebral α-Syn is required to accomplish its physiological role at the synapse (*20*,*21*). Titration of excessive α-Syn levels in a non-invasive manner would thus be beneficial in treating a chronic neurodegenerative disease like PD. Specifically, an orally available drug capable of mitigating α-Syn toxicity could offer a

72 minimally invasive approach, a feature particularly important in treating a chronic illness. A
73 pooled RNAi screen investigating modifiers of α-Syn levels identified cyclin-dependent kinase 14
74 (CDK14, a.k.a. PFTK1) as a robust regulator of α-Syn in human neurons and *in vivo* (*22*). CDK14
75 is a brain expressed protein kinase with a largely unknown biological function (*23*). Its expression
76 is upregulated in certain cancers, such as esophageal and colorectal cancer, for which it has
77 generated attention as a therapeutic target (*24*,*25*). In fact, this has led to the recent development
78 of FMF-04-159-2, a potent, covalent inhibitor of CDK14 (*26*).

79 Since reducing CDK14 leads to a mild reduction in endogenous α-Syn levels (*22*), we
80 hypothesize that genetic and pharmacological inhibition of CDK14 reduces α-Syn pathology and
81 PD-like phenotypes in mice and human cells. To test this hypothesis, we analyzed PD-like features
82 in two PD mouse models (mice injected with preformed α-Syn fibrils, and α-Syn transgenic mice)
83 with partial or full KO of *Cdk14*. Furthermore, using the recently developed specific CDK14
84 inhibitor, we tested if the pharmacological inhibition of CDK14 is sufficient to decrease α-Syn
85 levels in rodent and human neurons. In summary, we show that decreasing CDK14 prevents α-Syn
86 accumulation and ameliorates its downstream pathological consequences.

87

88 **RESULTS**

89 **CDK14 ablation ameliorates motor impairment and α-Syn pathology in PFF-injected mice**

90 Since PD is a chronic disease, inhibition of a candidate modifier would have to be safe, long term.
91 We first tested the level of expression and consequence of depletion of Cdk14 in vivo. We found
92 that Cdk14 was highly expressed in the brain (**fig. S1A**) and that Cdk14 nullizygous mice were
93 viable, fertile, and exhibited normal brain morphology (*27*). We next asked whether silencing
94 *Cdk14* is sufficient to mitigate behavioral and histological phenotypes observed in mice injected

95 with pathogenic α-Syn pre-formed fibrils (mouse PFFs; **Fig. 1A** and **B**; **fig. S1B** and **S2A**). Six
96 months following intrastriatal injection of α-Syn PFFs, there is a stereotypic brain-wide
97 accumulation of pS129 α-Syn – a marker of human synucleinopathies – in addition to SN DaNs
98 loss and mild motor impairments (*28–30*). In our experimental paradigm, six months after PFF
99 injection (at an age of 12 months), we found that PFF injected WT mice exhibited reduced forelimb
100 force generation in the grip strength test when compared to their saline-treated counterparts ($P <$
101 $0.001$, Fig. 1B), similar to what has been previously reported (*29*,*30*). In contrast, the PFF-induced
102 weakening of grip strength was not observed in *Cdk14*$^{+/-}$ or in *Cdk14*$^{-/-}$ mice. We did not observe
103 PFF-mediated changes (in any genotype tested) in the other 8 behavioral tests conducted (including
104 tests for cognitive and motor function). Furthermore, we noted that saline-injected *Cdk14*$^{+/-}$ and
105 *Cdk14*$^{-/-}$ mice consistently performed like their WT counterparts in each test, suggesting that
106 chronic Cdk14 reduction is not deleterious to the brain (**fig. S2A**).
107

108 **Cdk14 loss lowers signal of cerebral pS129 α-Syn reactivity after intrastriatal PFF injection**
109 We next turned to histology to determine the relative pathological burden of accumulated α-Syn
110 throughout the brain of mice injected with PFFs. We stained for synucleinopathy-linked pS129 α-
111 Syn in the brain of WT mice and found high amounts of pS129 α-Syn-positive cells in the PFF-
112 injected hemisphere (ipsilateral to the injection, IL), which were absent in saline-injected controls
113 ($P < 0.01$, data not shown). We then mapped the distribution of α-Syn pathology at three different
114 rostrocaudal levels near the injection site (relative to bregma: +0.98 mm, +0.26 mm and -1.34 mm)
115 and found an overall blunting of pS129 α-Syn-positive pathology in the PFF-injected *Cdk14*$^{+/-}$ and
116 *Cdk14*$^{-/-}$ mice when compared to their WT littermates (**Fig. 1C**). This was particularly evident IL
117 at the level of the somatomotor cortex (bregma +0.26 mm) and in other areas of the cortex (**Fig.**

118 **1C**). Previous reports have shown that α-Syn PFFs can induce nigrostriatal degeneration over time
119 (*28–30*). We stained for tyrosine hydroxylase (TH) at the injection site in the striatum but did not
120 observe a decrease of TH+ dopamine fibers in mice injected with PFFs (**fig. S2B**).
121

122 **Loss of Cdk14 mitigates PD-associated phenotypes in mice overexpressing human α-Syn**

123 We next asked whether partial loss of Cdk14 is sufficient to reduce α-Syn-induced phenotypes in
124 a more aggressive model of synucleinopathy. To do so, we crossed *Cdk14* heterozygous mice
125 (*Cdk14*$^{+/-}$) to wildtype (WT) or to α-Syn-overexpressing transgenic (*mThy1-SNCA*, a.k.a. "*α-Syn*
126 *TG*") mice (**Fig. 2A**) (*31*,*32*). These mice exhibit a 3-5-fold overexpression of human α-Syn and
127 exhibit a host of behavioral and neuropathological features reminiscent of PD within a few months
128 of age (*32*). We only examined male mice as the *α-Syn TG* transgene is located on the X
129 chromosome leading to X-inactivation and mosaic phenotypes in female mice. We tested whether
130 reduction of Cdk14 affects PD-like behavioral symptoms in 3-month-old *α-Syn TG* mice (**Fig. 2**).
131 We found that, in every test assayed, *α-Syn TG* mice exhibited strong motor deficits when
132 compared to their WT littermates (**Fig. 2B, C** and **D**). In the pole test, which is routinely used to
133 measure PD-like motor impairment in mice (*33*,*34*), we observed that mice harboring both the *α-*
134 *Syn TG* allele and a loss of function *Cdk14* allele (*α-Syn TG; Cdk14*$^{+/-}$) did not display any motor
135 dysfunction (**Fig. 2B**). This finding is particularly interesting given the high degree of α-Syn
136 overexpression compared to the modest reduction (50%) of Cdk14. In the beam break and nesting
137 tests *α-Syn TG; Cdk14*$^{+/-}$ mice displayed similar phenotype manifestations as their *α-Syn TG*
138 littermates (**Fig. 2C** and **D**).

139 We then measured the levels of α-Syn and phosphorylated α-Syn (pS129) isolated from
140 hemibrains of 5-month-old mice (**Fig. 2E**). The reduction of Cdk14 induced a surprising increase

141 in pS129 α-Syn levels in the soluble fraction of *α-Syn TG mice*, without affecting total α-Syn
142 dosage. However, in the insoluble protein fraction of this PD mouse line, Cdk14 loss did not alter
143 pS129 α-Syn levels. Instead Cdk14 loss led to a mild, yet significant reduction of total α-Syn.
144 These data suggest that reducing Cdk14 alters α-Syn metabolism, resulting in a net decrease of
145 aggregated α-Syn protein levels in the diseased mouse brain.
146

147 **Decreasing Cdk14 mitigates neurodegeneration in mice overexpressing human α-Syn**

148 *α-Syn TG* mice develop cortical and hippocampal cell loss as well as corresponding astrogliosis
149 and pS129 α-Syn accumulation (*31*,*35–37*) . We asked whether a 50% reduction of Cdk14 would
150 be sufficient to alter brain pathologies in 5-month-old *α-Syn TG* mice. We found that α-Syn
151 overexpression induced robust neuronal loss in the hippocampus (CA3 region) and cortex (Layer
152 V). In contrast, double mutant (*α-Syn TG; Cdk14*$^{+/-}$) littermates did not develop this level of
153 neurodegeneration in these brain regions (**Fig. 3A** and **B**). We measured the presence of aggregate-
154 associated α-Syn species via pS129 α-Syn staining and the degree of astrogliosis via GFAP
155 staining. We found that *α-Syn TG* mice developed pS129-positive α-Syn pathology and
156 astrogliosis, regardless of the *Cdk14* genotype (**fig. S3A** and **B**).
157

158 **Knockdown of CDK14 decreases α-Syn and pS129 α-Syn levels in human neurons**

159 Having observed the benefits of Cdk14 depletion in two mouse models of PD with different
160 degrees of α-Syn pathology, we next tested whether this benefit translates to human neurons. We
161 infected DaNs derived from a PD patient carrying an A53T mutation in α-Syn (*38*) as well as its
162 isogenic control with lentiviruses carrying Cas9/sgRNAs against *CDK14*. Neurons infected with
163 sgRNAs targeting either exon 3 (E3) or exon 8 (E8) of *CDK14*, exhibited approximately 50% of

164 the CDK14 levels of the control cultures (**Fig. 3C**). We found that A53T mutant cells showed a
165 marked increase of pS129 α-Syn compared to isogenic controls and, in parallel, PD neurons with
166 silenced *CDK14* exhibited significantly lower pS129 levels (**Fig. 3C**).
167

168 **Pharmacological targeting of CDK14 decreases α-Syn levels and mitigates its pathogenic**
169 **accumulation**

170 As kinases are typically druggable targets which can be inhibited in non-invasive ways (*39*), we
171 next asked whether CDK14 pharmacological inhibition would be a tractable route for decreasing
172 α-Syn levels. We used a recently developed CDK14 covalent inhibitor (FMF-04-159-2) (*26*) to
173 test whether acute depletion of CDK14 decreased α-Syn levels. We found that in HEK293T cells,
174 CDK14 inhibition induced a strong reduction in endogenous α-Syn protein levels (**Fig 4A**). We
175 asked whether CDK14 inhibition-induced α-Syn clearance was mediated by the ubiquitin
176 proteasome system (UPS) or autophagy. We found that blocking the UPS or autophagy did not
177 affect the reduction of α-Syn dosage, induced by CDK14 inhibition (**fig. S3C**). Rather, blocking
178 CDK14 resulted in decreased *SNCA* transcript levels. Moreover, we observed that CDK14 itself
179 was being cleared via the UPS. We next asked if CDK14 inhibition decreases α-Syn levels in
180 hESC-derived cortical neurons. CDK14 inhibition caused a dose-dependent reduction in total α-
181 Syn concentration by ELISA (**Fig. 4B)**. Lastly, we tested whether application of this inhibitor was
182 sufficient to block α-Syn pathology in rat primary neuronal cultures treated with α-Syn PFFs. We
183 found that Cdk14 inhibition markedly reduced the PFF-induced elevation of high molecular weight
184 α-Syn species over a five-day period (**Fig. 4C**). Thus, pharmacological treatment of isolated human
185 neurons or PFF-challenged rat neurons with a CDK14 inhibitor showed consistent reduction in α-
186 Syn protein.
187

188 **DISCUSSION**

189 α-Syn is increasingly considered a valid experimental therapeutic target for PD, based on clinical
190 genetic and neuropathological evidence, as well as animal and cell culture studies. *SNCA* gene
191 mutations or amplifications resulting in α-Syn pathology are tightly linked to PD pathogenesis.
192 Moreover, α-Syn is a major constituent of Lewy-like structures, the pathological hallmark of PD
193 and related synucleinopathies. Thus, targeting α-Syn has been a major thrust in the pharmaceutical
194 realm. One aspect of α-Syn pathology that has been difficult to overcome is the notion that different
195 states of its post-translational modification or aggregation differentially affect disease
196 pathogenesis: a clear image has yet to emerge as to the real culprit of α-Syn toxicity. Although
197 novel strategies such as anti-sense oligonucleotides, immunotherapy and small molecule inhibitors
198 of α-Syn aggregation are being explored (*40*), finding a target that can be pharmacologically
199 inhibited still holds potential as a minimally invasive and simple strategy to lower α-Syn levels –
200 especially when such treatment course would be made over several decades. Indeed, a growing
201 body of evidence suggests that α-Syn may play a role not only at the presynaptic space, but also
202 in the immune system (*41–43*). Therefore, careful titration of its levels may be more clinically
203 pertinent. As a result, we asked whether candidates that are more amenable to traditional
204 pharmacology (e.g. kinases) could regulate α-Syn dosage, irrespective of its aggregation status.
205 Our previous studies identified a handful of these modifiers including TRIM28 and DCLK1
206 (*8*,*22*,*36*,*44*). Here, we study a heretofore unexplored target for disease modification in pre-clinical
207 models of PD: CDK14.

208 Building on our initial identification of CDK14 as a potential regulator of α-Syn levels (*22*),
209 we show that reduction of CDK14 is well tolerated and causes a reduction in pathogenic α-Syn
210 accumulation in murine and human models of synucleinopathy. Genetic suppression of *Cdk14*
211 ameliorates the accumulation of pathologically linked pS129 α-Syn in the cortex of PFF-injected

212 mice and halts the development of PD-related motor defects. Moreover, we show that halving
213 Cdk14 in the brains of α-Syn overexpressing mice is sufficient to blunt the development of PD-
214 associated neurodegenerative phenotypes. Importantly, the genetic reduction of CDK14 in DaNs
215 derived from an individual with synucleinopathy shows equal promise in preventing phenotypic
216 development. Lastly, we show that a newly developed CDK14 inhibitor, FMF-04-159-2,
217 effectively inhibits CDK14, decreases α-Syn levels in hESC-derived human neurons, and mitigates
218 PFF-induced α-Syn pathology in rat cortical neurons. Collectively, these results show that CDK14
219 is a pharmacologically tractable target for synucleinopathy.

220 We found that while the net effect of decreasing CDK14 on reducing α-Syn levels and its
221 associated phenotypes were consistent, its effect on α-Syn phosphorylation was context-
222 dependent. For instance, genetic reduction of CDK14 resulted in decreased pS129 α-Syn in both
223 the PFF model as well as the human DaNs derived from the *SNCA-A53T* carrier. In contrast, partial
224 reduction of Cdk14 resulted in an increase in soluble pS129 α-Syn in the *α-Syn TG* line, despite
225 decreasing total aggregated α-Syn and blunting neurodegenerative phenotypes. We surmise that
226 Cdk14 mediates its effect toward α-Syn not directly via its phosphorylation. Indeed, we could not
227 detect any kinase activity of recombinant CDK14 toward wild-type α-Syn *in vitro* (data not
228 shown). Thus, we hypothesize that loss or inhibition of CDK14 causes a decrease in α-Syn through
229 an unknown mediator, affecting maintenance of *SNCA* transcript and α-Syn protein levels. Future
230 studies will help refine the mechanism whereby CDK14 regulates α-Syn.

231 Our results examining the genetic and pharmacological reduction of CDK14 in PD models
232 pioneer future pre-clinical studies. In all behavioral experiments conducted, Cdk14$^{-/-}$ mice were
233 indistinguishable from WT mice (**Fig 1B** and **fig S1**), implying that *Cdk14* loss is not deleterious
234 *in vivo*. This is supported by human genetics where loss of *CDK14* appears to be well tolerated

235 (probability of loss of function intolerance [pLI] = 0; gnomAD database, CDK14 | gnomAD
236 v2.1.1), (*45*)). Moreover, the activity of the CDK14 inhibitor in human neurons appears to be high,
237 affecting CDK14 (and thus α-Syn metabolism) in the nanomolar range. While FMF-04-159-2 has
238 yet to be tested in animal models, our cell culture experiments provide proof-of-principle for its
239 potential role in the reduction of α-Syn pathology. Further preclinical experiments will address the
240 safety of FMF-04-159-2 in animals and test whether the drug rescues PD-like models of
241 synucleinopathies; potentially paving the way for its application in human subjects.

242 In sum, we show that CDK14 inhibition causes a decrease total α-Syn concentrations under
243 both *ex vivo* and *in vivo* conditions and consequently ameliorates α-Syn-driven phenotypes in
244 mouse and human PD models. Given the strong evidence linking α-Syn levels to PD pathogenesis,
245 we conclude that targeting CDK14 function holds promise as a potentially disease-modifying
246 approach to treat PD.

247

248 **MATERIALS AND METHODS**

249 **Study design**

250 The objective of this study was to analyze whether reduction of CDK14 decreases α-Syn pathology
251 *in vitro* and *in vivo*. To test if Cdk14 reduction mitigates α-Syn-induced toxicity in PD mouse
252 models, we injected preformed mouse α-Syn fibrils (PFFs) in the brains of *Cdk14*$^{+/-}$, *Cdk14*$^{-/-}$ and
253 WT littermate mice. In addition, we combined mice with genetic reduction of *Cdk14* with mice
254 overexpressing full-length human α-Syn to test whether genetic reduction of *Cdk14* ameliorates
255 PD-like characteristics. Dosage of α-Syn protein was analyzed in human neurons from *SNCA A53T*
256 carriers with reduced CDK14 levels. Furthermore, we asked if pharmacological inhibition of
257 CDK14 affects α-Syn levels in rodent and human cells and applied the CDK14 inhibitor FMF-04-

258 159-2 to cultured rat and hESC-derived human cortical neurons. Sample size was established prior
259 to study onset and were generally picked based on previous data from the literature using these
260 models. All procedures with mice were performed in accordance with the guidelines of the
261 Canadian Council on Animal Care and stipulations of the Ethics Board and the Animal Care
262 Committee at the University of Ottawa.

263

264 **Mouse strains**

265 *Cdk14*$^{+/-}$ mice were generated by the Gene Targeting and Transgenic Facility of Texas A&M
266 Institute for Genomic Medicine (TIGM), on a mixed (129/SvEvBrd x C57BL/6) background (as
267 described previously (*27*). *Cdk14*$^{+/-}$ mice were backcrossed 14 times to the C57Bl/6NCrl
268 background prior to experimentation (PFF or genetic interaction). *Cdk14*$^{+/-}$ mice were paired to
269 generate *Cdk14*$^{-/-}$ mice. Since the *α-Syn TG* transgene is located on the X chromosome (*32*), *α-Syn*
270 *TG; Cdk14*$^{+/-}$ X chromosomal females were paired with *Cdk14*$^{+/-}$ males. Resulting WT, *α-Syn TG*,
271 *Cdk14*$^{+/-}$ and *α-Syn TG; Cdk14*$^{+/-}$ males were used for experimental procedures. Only males were
272 used for experiments as female mice undergo X chromosome inactivation, resulting in variable
273 phenotypes. Behavioral experiments were performed on 3-month-old mice.

274

275 **Stereotactic PFF injections**

276 Endotoxin-free recombinant mouse α-Syn fibril preparations were stored at -80ºC before usage
277 (*46*,*47*). On the day of the stereotactic injections, fibrils were thawed and sonicated in a sonicator
278 water bath to generate PFFs (Covaris S220, 18 W peak incident power, 20% duty factor, 50 cycles
279 per burst, 150 seconds). For transmission electron microscopy (TEM) analysis (Transmission
280 Electron Microscopy Core Facility, University of Ottawa) 0.2 mg/mL PFF samples were stained

281 with Uranyl Acetate and imaged on a FEI Tecnai G2 Spirit Twin TEM. 6-month-old mice were
282 deeply anesthetized with isoflurane, and 1 μL PFFs (5 mg/mL) or sterile saline (0.9% NaCl) was
283 unilaterally delivered into the dorsal striatum of the right hemisphere at these coordinates relative
284 to bregma: -2 mm medial-lateral; +0.2 mm antero-posterior and -2.6 mm dorso-ventral. Injections
285 were performed using a 2 μL syringe (Hamilton, Reno, NV, USA) at a rate of 0.1 μL/min with the
286 needle left in place for at least 3 minutes before its slow withdrawal. After surgery, animals were
287 monitored, and post-surgical care was provided. Behavioral experiments were performed 6 months
288 post injection, followed by the collection of the brains at 7 months post injection.
289

290 **Behavioral experiments**

291 Grip strength tests were performed by holding the mice at an automatic grip strength meter
292 (Chatillon DFE II, Columbus Instruments) allowing them to grip the grid of the device with their
293 fore- and hindlimbs. Then, mice were gently pulled back by their tail until they released the grip.
294 Force exerted by the mouse during its removal from the grid, as measured by gram force (g), was
295 evaluated 5 times per mouse. For nesting behavior tests, mice were singly caged overnight (16
296 hours) with a 5x5cm cotton nestlet in a clean cage. Produced nests were scored on a scale from 1-
297 5 as previously described (*48*). For beam break tests single mice were placed in the testing
298 apparatus (Omnitech Electronics) for 24 hours with standard rodent chow and water *ad libitum*.
299 Locomotion is presented as distance travelled. Pole tests were performed by placing the mice on
300 the top of a vertical pole (8 mm diameter and 55 cm height) with a rough surface. Mice were placed
301 with their head facing the room ceiling and the time required for turning was recorded. The mean
302 time to turn was calculated from 5 consecutive trials for each mouse.
303

304 **Tissue harvesting and processing**

305 For biochemical approaches with hemibrains from 5-month-old *α-Syn TG Cdk14*$^{+/-}$ *mice and their*
306 *littermates*, mice were anesthetized with isoflurane (Fresenius Kabi, CP0406V2), and decapitated.
307 Brains were isolated and hemibrains were lysed 1:4 (w/v) in NETN buffer (250 mM NaCl, 5 mM
308 EDTA pH 8, 0.5% NP-40, 50 mM Tris-HCL, pH 8 in dd$H_2O$) with protease (GenDEPOT, P3100)
309 and phosphatase inhibitors (GenDEPOT, P3200) using Dounce homogenizers. Lysates were
310 cleared by centrifugation at 18,000 x *g* for 20 minutes at 4°C. Cleared lysates were transferred to
311 a new, low protein binding tube, and the pellets were frozen at -80°C for subsequent analysis. To
312 isolate insoluble proteins, pellets were thawed and resuspended in 88% formic acid 1:1 (w/v).
313 Samples were left to incubate for 1 hr at room temperature, then diluted to 22 % formic acid content
314 with PBS. Samples were dried overnight at 60 °C in an Eppendorf Vacufuge concentrator. Dried
315 protein was resuspended in phosphate-buffered saline (PBS) with protease and phosphatase
316 inhibitors at 1:4 (w/v) based on the initial hemibrain weight. Samples were sonicated at 20 % 10
317 sec ON, 10 sec OFF for 4 minutes total time, using an FB120 sonicator (Fisher Scientific) with Cl-
318 18 probe (Qsonica), while kept on ice.

319 For immunohistology with paraffin sections, mice were anesthetized with 120 mg/kg Euthanyl
320 (DIN00141704) and intracardially perfused with 10 mL of PBS, followed by 20 mL of 10 %
321 Buffered Formalin Phosphate (Fisher Scientific, SF100-4). Brains were isolated and fixed in 10 %
322 Buffered Formalin Phosphate at 4°C for at least 24 hours. After dehydration by 70 %, 80 %, 90 %
323 and 100 % ethanol and clearing by Xylenes, brains were infiltrated and embedded in paraffin
324 (Louise Pelletier Histology Core Facility, University of Ottawa). Brains were sectioned at 5 µm.

325

326 **SDS-PAGE and mouse protein immunoblots**

327 4X Laemmli buffer (Bio-Rad, 1610747) with 20 % 2-mercaptoethanol (Bio-Rad, 1610710) was
328 added to cleared protein and boiled at 95 °C for 5 minutes. Protein samples were loaded on a 12
329 % SDS-PAGE gel in the Mini-PROTEAN Tetra Cell (Bio-Rad, 165-8000). Protein was then
330 transferred to a 0.2 µm nitrocellulose membrane (Bio-Rad, 1620112) using the Mini Trans-Blot
331 Electrophoretic Transfer Cell (Bio-Rad, 1703930) in Tris-Glycine buffer with 10 % methanol
332 (Fisher Scientific, A412P) at 340mA for 90 minutes at 4 °C. Membranes were then blocked in 5
333 % milk in 1X TBS-T for 1hr at room temperature followed by overnight incubation in primary
334 antibody against pSer129 α-Syn (1:2,000, Abcam, 51253), α-Syn (1:2,000, BD Biosciences,
335 610787), CDK14 (1:500, Santa Cruz, sc50475) and GAPDH (1:40,000, Proteintech, 60004-1-Ig)
336 diluted in 2% BSA, 0.02% $NaN_3$ in 1X TBS-T. Next, membranes were washed in TBS-T, followed
337 by incubation in secondary antibody (peroxidase-conjugated donkey anti-rabbit IgG, Cedarlane,
338 711-035-152 or donkey anti-mouse IgG, Cedarlane, 715-035-150, both at 1:10,000 diluted in 5%
339 milk in TBS-T) for 1 hour at room temperature. Membranes were washed again in TBS-T, bathed
340 in enhanced chemiluminescent reagent (Bio-Rad, 1705061), imaged using the ImageQuant LAS
341 4100 Imaging system (GE) and quantified using Image Lab 6.1 software (Bio-Rad Laboratories).
342

343 **Immunohistology**

344 For Diaminobenzidine (DAB) antibody staining, paraffin sections were deparaffinized in xylenes
345 and rehydrated in a series of decreasing ethanol (100 %, 90 %, 70 %, 50 %) followed by antigen
346 retrieval in sodium citrate buffer (2.94 g sodium citrate, 0.5 mL Tween-20 in 1 L PBS, pH6) at
347 95°C for 20 min and quenching of endogenous peroxidase with 0.9 % $H_2O_2$ in PBS for 10 min.
348 Sections were blocked in blocking buffer (0.1 % Triton X-100, 10 % normal horse serum in PBS)
349 and incubated in primary antibody (pSer129 α-Syn, 1:500, Abcam, 51253 or tyrosine hydroxylase,

350 1:1,000, Sigma-Aldrich, AB152) overnight at 4 ºC. Then, sections were incubated in secondary
351 antibody (donkey anti-rabbit biotin-conjugated, Jackson ImmunoResearch, 711-065-152, 1:250 in
352 blocking buffer) for 2 hours and tertiary antibody solution (streptavidin-horseradish peroxidase
353 conjugated, 1:500 in blocking buffer, Sigma-Aldrich, RPN1231V) for 2 h before being exposed to
354 DAB (Vector, SK-4100) for 10 minutes. Hematoxylin counterstaining was conducted using the
355 H&E Staining Kit (Abcam, ab245880) as per manufacturer's instructions. Stained sections were
356 dehydrated in a series of ethanol and xylenes solutions, followed by mounting sections with
357 Permount (Fisher Scientific, SP15-100).
358 For immunofluorescence antibody staining, after the deparaffinization/dehydration, antigen
359 retrieval and blocking, sections were incubated in primary antibody (NeuN, 1:500, EMD
360 Millipore, MAB377 or GFAP, 1:1,000, Synaptic Systems, 173 004) in blocking buffer overnight
361 at 4ºC. Next, sections were incubated in secondary antibody (donkey anti-mouse IgG (H+L) Alexa
362 Fluor™ 568, Thermo Fisher Scientific, A10037, for NeuN and goat anti-guinea pig IgG (H+L)
363 Alexa Fluor™ 488, for GFAP) together with DAPI (Sigma-Aldrich, D9542) for 1 hour at RT,
364 followed by mounting sections with fluorescence mounting medium (Agilent, S302380-2).
365 Brightfield and epifluorescence micrographs were acquired using an Axio Scan Z1 Slide Scanner
366 (20x objective, Louise Pelletier Histology Core Facility) and a Zeiss AxioImager M2 (10x
367 objective, Cell Biology and Image Acquisition Core Facility, University of Ottawa) and analyzed
368 using ImageJ (National Institute of Health, 1.52p) with 2-3 sections per mouse by a blinded
369 investigator. Heatmaps were generated by counting pS129 α-Syn positive cells in defined regions
370 of the brain (http://atlas.brain-map.org), normalized to the area occupied by the region and
371 resulting cell densities were expressed as hues of red.
372

373 **Cell culture**

374 Cells were kept at 37 °C, 5 % $O_2$, 10 % $CO_2$. HEK293T cells (ATCC, CRL-3216) were cultured
375 in Dulbecco's modified Eagle's medium (DMEM, Wisent Bioproducts, 319-015-CL),
376 supplemented with 10% FBS (Sigma-Aldrich, F1051) and antibiotic/antimitotic (Thermo
377 Scientific, 15240062).

378

379 **hiPSC culture, neuronal differentiation, and Cas9-mediated gene editing**

380 hiPSC isogenic lines (Female) and hESC isogenic lines (Male) were generated as described by
381 (*38*). Genotypes of hESC-derived WT, A53T, and E46K as well as hiPSC-derived Corrected and
382 A53T cell lines were confirmed by restriction digest of genomic DNA (*38*). hiPSCs were cultured
383 as previously described (*49*) with slight modifications. Briefly, pluripotent cells were plated in
384 mTeSR (Stem Cell Technologies) and media was changed daily. The colonies were manually
385 passaged weekly. Differentiation of hPSCs into A9-type DaNs was performed by following a floor
386 plate differentiation paradigm (*49*,*50*). Immediately preceding differentiation, the colonies were
387 dissociated into a single cell suspension using HyQTase. hPSCs were collected and re-plated at
388 $4x10^4$ cells/$cm^2$ on Matrigel (BD)-coated tissue culture dishes for differentiation. Floor-plate
389 induction was carried out using hESC-medium containing knockout serum replacement (KSR),
390 LDN193189 (100 nM), SB431542 (10 μM), Sonic Hedgehog (SHH) C25II (100 ng/mL,
391 Purmorphamine (2 μM), Fibroblast growth factor 8 (FGF8; 100 ng/mL), and CHIR99021 (3 μM).
392 On day 5 of differentiation, KSR medium was incrementally shifted to N2 medium (25%, 50%,
393 75%) every 2 days. On day 11, the medium was changed to Neurobasal/B27/Glutamax
394 supplemented with CHIR. On day 13, CHIR was replaced with Brain Derived Neurotrophic Factor
395 (BDNF; 20 ng/mL), ascorbic acid (0.2 mM), Glial Derived Neurotrophic Factor (GDNF; 20

396 ng/mL), transforming growth factor beta 3 (TGFβ3; 1 ng/mL), dibutyryl cAMP (dbcAMP; 0.5
397 mM), and DAPT (10 μM) for 9 days. On day 20, cells were dissociated using HyQTase and re-
398 plated under high cell density $4x10^5$ cells/$cm^2$ in terminal differentiation medium (NB/B27 +
399 BDNF, ascorbic acid, GDNF, dbcAMP, TGFβ3 and DAPT) also referred to as DA Neuron (DAN)-
400 Medium, on dishes pre-coated with poly-ornithine (15 μg/mL)/laminin (1 μg/mL)/fibronectin (2
401 μg/mL). Cells were differentiated for up to 60 DIV, with analysis being performed at DIV14, DIV
402 45 and/or DIV 60. At D10D and D14D or differentiation, hPSC cultures were transduced with
403 lentivirus containing Cas9 (lentiCRISPR v2, addgene, plasmid #52961) with the following
404 gRNAs: non-targeting (5'-CGCTTCCGCGGCCCGTTCAA-3'), CDK14 exon 3 (5'-
405 GCAAAGAGTCACCTAAAGTT-3') and exon 8 (5'-TGTGCAAAATATAACGCTGG-3').
406 From D10D-D14D media was supplemented with 0.1 μM compound E (AlfaAesar, J65131). At
407 D18D, cells were replated onto poly-ornithine (15 μg/mL)/laminin (1 μg/mL)/fibronectin (2
408 μg/mL) coated plates. Cells were maintained in DAN-medium (DMEM/F12, 200uM Ascorbic
409 Acid, 0.5 mM dbcAMP, 20 ng/mL BDNF, 20 ng/mL GDNF, 1 ng/mL TGFb3, and 1 % Anti-Anti)
410 for 6-7 weeks where lysates were then collected for protein analysis.
411

412 **hESC culture, neuronal differentiation and *in vitro* CDK14 inhibitor treatment**

413 Dishes for hESC cultures were coated with 0.15 mg/mL growth factor reduced Matrigel (Corning,
414 354230) in DMEM/F-12 (Thermo Fisher Scientific, 11320033) for 1 hour at room temperature
415 prior to cell seeding. H9 hESCs (WiCell, WA09) were seeded as colonies and maintained in
416 mTeSR Plus (StemCell Technologies, 05825). Neural progenitor cell (NPC) differentiation was
417 initiated when the hESC cultures reached 90% confluence, by replacing growth medium with
418 Knockout Serum Replacement (KSR) medium (414 mL Knockout-DMEM (Thermo Fisher

419 Scientific, 10829018), 75 mL Knockout-serum replacement (Thermo Fisher Scientific,
420 10828028), 5 mL Glutamax (Thermo Fisher Scientific, 35050061), 5 mL MEM-NEAA (Thermo
421 Fisher Scientific, 11140050), 500 µL 2-mercaptoethanol (Thermo Fisher Scientific, 21985023),
422 500 µL Gentamicin (Wisent Bioproducts 450-135), 10 µM SB431542 (Tocris, 1614) and 500 nM
423 LDN-193189 (Stemgent, 04-0074). Differentiation medium was replaced daily on days 4 and 5 by
424 75:25 KSR:N2 medium (486.5 mL DMEM/F-12 (Thermo Fisher Scientific, 11320033), 5 mL 15%
425 glucose, 5 mL N2 supplement (Thermo Fisher Scientific, 17502048), 500 µL 20 mg/mL human
426 insulin (Wisent Bioproducts, 511-016-CM), 2.5 mL 1M HEPES (Thermo Fisher Scientific,
427 15630080), 500 µL Gentamicin), on days 6 and 7 by 50:50 KSR:N2, on days 8 and 9 by 25:75
428 KSR:N2 and on days 10 and 11 by N2 medium containing 500 nM LDN-193189. On day 12,
429 differentiated NPCs were treated with Y-27632 (Tocris, 1254) for 4 hours, dissociated with
430 Accutase (Stemcell Technologies, 07922) and seeded into Matrigel coated dishes containing
431 Neural Induction Medium (NIM, 244 mL DMEM/F12, 244 mL Neurobasal medium (Thermo
432 Fisher Scientific, 21103049), 2.5 mL N2 Supplement, 5 mL B-27 Supplement (Thermo Fisher
433 Scientific, 17504044), 2.5 mL GlutaMAX™ (Thermo Fisher Scientific, 35050061), 125 µL 20
434 mg/mL human insulin, 500 µL 20 µg/mL FGF2 (StemBeads, SB500), 10 µL 1 mg/mL hEGF
435 (Millipore Sigma E9644) and 500 µL Gentamicin) for expansion. NPCs were passaged at full
436 confluence a minimum of one time before neuronal differentiation.

437 For NPC-neuronal differentiation culture dishes were coated with 0.001 % Poly-L-
438 ornithine (Millipore Sigma, P4957) at 4 °C overnight, followed by 25 µg/mL laminin (Millipore
439 Sigma, L2020) for 2 h at room temperature. NPCs were treated with Y-27632 for 4 hours,
440 dissociated with Accutase and seeded at a density of 20,000 cells/cm$^2$ in NIM. Neuronal
441 differentiation was initiated when NPCs reached 70% confluence by replacing growth medium

442 with neuronal differentiation medium (244 mL DMEM/F-12 medium, 244 mL Neurobasal
443 medium, 2.5 mL N2 supplement, 5 mL B27 supplement, 200 µL 50 µg/ml BDNF (Peprotech, 450-
444 02), 200 µL 50 µg/ml GDNF (Peprotech, 450-10), 250 mg dibutyryl cyclic-AMP (Millipore
445 Sigma, D0627), 500 µL 100 M L-ascorbic acid (FujiFim Wako Chemicals, 323-44822), and 500
446 µL Gentamicin). Cells were fed every 3 days for 18 days to obtain immature neuronal networks.
447 FMF-04-159-2 (R&D Systems, 7158) was dissolved in DMSO (Fisher Scientific, BP231) and
448 applied in cell culture medium to hESC-derived neurons for 72 hours and to HEK293T cells for
449 18 hours. HEK293T cells were treated with 500 nM of FMF-04-159-2 together with 200 nM of
450 Bafilomycin A1 (in DMSO, NEB, 54645S) or 1 µM of MG-132 (in DMSO, EMD Millipore,
451 474790) for 18 hours to inhibit autophagy or the UPS, respectively. For protein analysis cells were
452 washed with cold PBS, scraped, and collected in low protein binding microcentrifuge tubes
453 (Thermo Scientific, 90410). Cells were pelleted by centrifugation at 1,000 x g for 5 minutes at
454 4°C. The supernatant was aspirated, and the cells were lysed in cold RIPA buffer (50 mM Tris, pH
455 7.5, 150 mM NaCl, 0.1% SDS, 0.5% sodium deoxycholate; 1% NP-40, 5 mM EDTA, pH 8.0) with
456 protease and phosphatase inhibitors. Cell lysates were incubated on ice for 20 minutes, with
457 vortexing every 5 minutes. Lysates were centrifuged at 18,000 x *g* for 20 minutes at 4 °C to pellet
458 cell debris. Autophagic activity was monitored by immunoblots for LC3B (Novus Biologicals,
459 NB100-2220). Proteasome activity was monitored by immunoblots for poly-ubiquitinated proteins
460 (anti-ubiquitin P4D1, Cell Signaling Technology, 3136).
461

462 **RNA extraction and Reverse Transcription Quantitative PCR (RTqPCR)**

463 RNA from HEK293T cells was extracted using the RNeasy Mini Kit (Qiagen, 74106) following
464 the manufacturer's guidelines. cDNA was synthesized using the 5X All-in-One RT Master Mix

465 Kit (BioBasic, HRT025-10). RTqPCR was conducted using the Green-2-Go qPCR Master Mix
466 (BioBasic, QPCR004-S) with 25 ng DNA per reaction and primers targeting *GAPDH* (Forward:
467 5'-CGACCACTTTGTCAAGCTCA-3', Reverse: 5'-TTACTCCTTGGAGGCCATGT-3'),
468 *HPRT1* (Forward: 5'-GACCAGTCAACAGGGGACAT-3', Reverse: 5'-
469 GTGTCAATTATATCTTCCACAATCAAG-3') and *SNCA* (Forward: 5'-
470 ACCAAACAGGGTGTGGCAGAAG-3', Reverse: 5'- CTTGCTCTTTGGTCTTCTCAGCC-3').
471 Reactions were performed in a BioRad CFX96 thermocycler (protocol: 95 ºC for 5 minutes, 40
472 cycles of 95 ºC for 15 seconds and 60 ºC for 60 seconds, followed by melting curve). *SNCA* Ct
473 values were standardized to the average of *GAPDH* and *HPRT1* Ct values and *SNCA* expression
474 was displayed as fold change of the DMSO control.
475
476 **ELISA**
477 ELISA α-Syn protein quantification was performed as previously described (*41*,*51*). 384-well
478 MaxiSorp plates (Nunc, Inc) were coated with capturing antibody (α-Syn, BD Biosciences,
479 610787) diluted 1:500 in coating buffer ($NaHCO_3$ with 0.2 % NaN3, pH 9.6) overnight at 4 °C.
480 Following 3 washes with PBS/0.05 % Tween-20 (PBST), plates were blocked for 1 hour at 37 °C
481 in blocking buffer (1.125 % fish skin gelatin; PBS-T). After 3 washes, samples were loaded in
482 duplicates and incubated at RT for 2 hours. Biotinylated hSA4 antibody (in-house antibody) was
483 generated using 200 µg Sulfo-NHS-LC Biotin (Pierce), diluted 1:200 in blocking buffer and added
484 to the plate for 1 hour at 37 °C. Following 5 washes, ExtrAvidin phosphatase (Sigma E2636)
485 diluted in blocking buffer was applied for 30 min at 37 °C. Color development was carried out by
486 using fast-p-nitrophenyl phosphate (Sigma, N1891) and monitored at 405 nm every 2.5 min for up

487 to 60 min. Saturation kinetics were examined for identification of time point(s) where standards
488 and sample dilutions were in the log phase.
489
490 **Primary rat neurons, human α-Syn PFFs and protein analysis**
491 Cortical neurons were harvested from the E18 Sprague Dawley rat embryos (Charles River). The
492 harvested cortical tissue was digested using 17 U/mg Papain followed by mechanical dissociated
493 by gentle trituration through a glass flamed Pasteur pipet. The cells were seeded into plates coated
494 24 hours prior to dissection with Poly-D-Lysine (0.15 mg/mL). The cells were incubated at 37 °C,
495 7.5 % $CO_2$ until collection. Every 3 to 4 days, a 50% media change was performed (2 % B27
496 supplement, 1 % antibiotic/antimycotic, 0.7 % BSA Fraction V, 0.1 % β-mercaptoethanol in
497 HEPES-buffered DMEM/F12). Where required, cells were exposed to 100 nM FMF-04-159-2
498 (Bio-Techne, 7158/10) dissolved in DMSO, at 14 DIV, and again at the subsequent feed (18 DIV).
499 At 14 DIV, cells were exposed to either 1 μg/mL human α-Syn PFFs, or 1 μg/mL monomeric α-
500 Syn. Cell lysates were collected at D0 (no exposure), D1, D3, and D5 post PFF or monomeric
501 exposure. Human α-Syn protein was isolated from BL21-CodonPlus (DE3)-RIPL competent cells
502 transformed with pET21a-alpha-synuclein and purified by Reversed-phase HPLC. PFFs were then
503 generated as previously described (*52*). Purified α-Syn (5 μg/mL in PBS) was incubated at 37°C
504 with constant shaking for 7 days, then aliquot and stored at -80 °C. Prior to use, PFFs were thawed
505 and diluted in PBS, then subjected to sonication (20 % amplitude, 30 seconds; 1 second on, 1
506 second off) and added to neuronal media for exposure to neurons at a concentration of 1 μg/mL
507 for 24 hours. Following the incubation, cell lysates were collected in 150 μL ice-cold RIPA buffer
508 containing phosphatase and protease inhibitors (1 mM aprotinin, 1 mM sodium orthovanadate, 1
509 nM sodium fluoride, and 10 mM phenylmethylsulfonyl fluoride). Samples were homogenized

510 using a 18G needle, left on ice to rest for 15 minutes, and then centrifuged at 14,000 *g* to remove
511 any cellular debris. Using the BioRad DC Protein Assay kit, the protein concentration of each
512 sample was quantified following the manufacturers guidelines. SDS-PAGE was performed using
513 a 12.5 % resolving gels and a 4 % stacking gels, and gels were run for 15 minutes at 80 V followed
514 by approximately 1.5 hours at 110 V. The gels were transferred onto 0.2 μM nitrocellulose
515 membranes at 35 V and 4°C overnight. Following the transfer, the membranes were blocked for 1
516 hour at room temperature using blocking buffer (5 % non-fat dry milk in 1X PBS) with constant
517 agitation. Primary antibodies were prepared in blocking buffer containing 0.1 % Tween20 and
518 were probed overnight at 4 °C under constant agitation (CDK14, 1:1,000, Santa Cruz, sc50475,
519 TH, 1:1,000, Pel Freeze, P40101, a-Syn, 1:1,000, BD, BD 610787, pS129 a-Syn, 1:500, abcam,
520 ab51253, β-Actin, 1:1,000, rabbit, Biolegend, 622101 or mouse, Sigma, A5411, βIII-Tubulin,
521 1:5,000, rabbit, Biolegend, 802001). Following primary antibody incubation, membranes were
522 rinsed using 1XPBS containing 0.1 % Tween20 and subsequently re-blocked using the blocking
523 buffer. The membranes were then probed with secondary antibody for 1 hour at RT in blocking
524 buffer containing 0.1 % Tween20 (Goat anti-Mouse IgG (H+L) Secondary Antibody, HRP
525 (Thermo Fisher Scientific, 31430); Goat anti-Rabbit IgG (H+L) Secondary Antibody, HRP
526 (Thermo Fisher Scientific, 31460); Li-Cor infrared conjugated secondary/ IRDye 800RD Donkey
527 anti-Rabbit IgG antibody (LI-COR Biosciences, 926-32211) at dilutions of 1:2,000). The
528 membranes were rinsed to remove any residual blocking buffer using 1X PBS containing 0.1 %
529 Tween20. If HRP-conjugated secondary antibodies were used, membranes were probed for 5
530 minutes with clarity Western enhanced chemiluminescence blotting substrate (Bio-Rad) and
531 visualized with photosensitive film. For LiCOR-secondary antibodies, membranes were visualized
532 with a LiCOR Odyssey Fc.

533

534 **Statistics**

535 Statistical analysis was performed using GraphPad Prism version 9.2.0. Quantified data are
536 visualized as mean + standard error of the mean. Unpaired student's *t* tests were used for two-
537 group comparisons. Data affected by one or two factors were analyzed by one-way or two-way
538 analysis of variance (ANOVA), respectively, followed by Bonferroni *post hoc* comparisons
539 (unless otherwise stated in the figure legend) when at least one of the main factors or the interaction
540 was significant. A significance level of 0.05 was accepted for all tests. Asterisks mark $P$ values ≤
541 0.05 (*), ≤ 0.01 (**), ≤ 0.001 (***), or ≤ 0.001 (****).

542

543 **References and Notes**


544 1. Selvaraj S, Piramanayagam S. Impact of gene mutation in the development of Parkinson's
545 disease. Genes Dis. 2019;6(2):120–8.
546 2. Mhyre TR, Boyd JT, Hamill RW, Maguire-Zeiss KA. Parkinson's disease. Subcell
547 Biochem. 2012;65:389–455.
548 3. Sveinbjornsdottir S. The clinical symptoms of Parkinson's disease. J Neurochem.
549 2016;139:318–24.
550 4. Mazzoni P, Shabbott B, Cortés JC. Motor control abnormalities in Parkinson's disease.
551 Cold Spring Harb Perspect Med. 2012;2(6):1–17.
552 5. Berardelli A, Rothwell JC, Thompson PD, Hallett M. Pathophysiology of bradykinesia in
553 Parkinson's disease. Brain. 2001 Nov;124(11):2131–46.
554 6. Mor DE, Ischiropoulos H. The Convergence of Dopamine and α-Synuclein: Implications
555 for Parkinson's Disease. J Exp Neurosci. 2018 Mar;12:1179069518761360–
556 1179069518761360.
557 7. Fujiwara H, Hasegawa M, Dohmae N, Kawashima A, Masliah E, Goldberg MS, et al. α-
558 Synuclein is phosphorylated in synucleinopathy lesions. Nat Cell Biol [Internet].
559 2002;4(2):160–4. Available from: https://doi.org/10.1038/ncb748
560 8. Vázquez-Vélez GE, Gonzales KA, Revelli J-P, Adamski CJ, Alavi Naini F, Bajić A, et al.
561 Doublecortin-like Kinase 1 Regulates α-Synuclein Levels and Toxicity. J Neurosci
562 [Internet]. 2020;40(2):459. Available from:
563 http://www.jneurosci.org/content/40/2/459.abstract
564 9. Rousseaux MWC, Shulman JM, Jankovic J. Progress toward an integrated understanding
565 of Parkinson's disease [version 1; peer review: 2 approved]. F1000Research [Internet].
566 2017;6(1121). Available from: http://openr.es/9uu
567 10. Campêlo CL das C, Silva RH. Genetic Variants in SNCA and the Risk of Sporadic

Parkinson's Disease and Clinical Outcomes: A Review. Parkinsons Dis [Internet]. 2017/07/11. 2017;2017:4318416. Available from: https://pubmed.ncbi.nlm.nih.gov/28781905

11. Singleton AB, Farrer M, Johnson J, Singleton A, Hague S, Kachergus J, et al. α-Synuclein Locus Triplication Causes Parkinson's Disease. Science (80- ) [Internet]. 2003;302(5646):841. Available from: http://science.sciencemag.org/content/302/5646/841.abstract
12. Gründemann J, Schlaudraff F, Haeckel O, Liss B. Elevated α-synuclein mRNA levels in individual UV-laser-microdissected dopaminergic substantia nigra neurons in idiopathic Parkinson's disease . Nucleic Acids Res [Internet]. 2008 Mar 10;36(7):e38–e38. Available from: https://doi.org/10.1093/nar/gkn084
13. Feany MB, Bender WW. A Drosophila model of Parkinson's disease. Nature [Internet]. 2000;404(6776):394–8. Available from: https://doi.org/10.1038/35006074
14. Masliah E, Rockenstein E, Veinbergs I, Mallory M, Hashimoto M, Takeda A, et al. Dopaminergic Loss and Inclusion Body Formation in α-Synuclein Mice: Implications for Neurodegenerative Disorders. Science (80- ) [Internet]. 2000;287(5456):1265. Available from: http://science.sciencemag.org/content/287/5456/1265.abstract
15. Lakso M, Vartiainen S, Moilanen A-M, Sirviö J, Thomas JH, Nass R, et al. Dopaminergic neuronal loss and motor deficits in Caenorhabditis elegans overexpressing human α-synuclein. J Neurochem [Internet]. 2003 Jul 1;86(1):165–72. Available from: https://doi.org/10.1046/j.1471-4159.2003.01809.x
16. Chu Y, Kordower JH. Age-associated increases of α-synuclein in monkeys and humans are associated with nigrostriatal dopamine depletion: Is this the target for Parkinson's disease? Neurobiol Dis [Internet]. 2007;25(1):134–49. Available from: http://www.sciencedirect.com/science/article/pii/S0969996106002191
17. Polymeropoulos MH, Lavedan C, Leroy E, Ide SE, Dehejia A, Dutra A, et al. Mutation in the alpha-synuclein gene identified in families with Parkinson's disease. Science. 1997 Jun;276(5321):2045–7.
18. Stefanis L. α-Synuclein in Parkinson's Disease. Cold Spring Harb Perspect Med [Internet]. 2012 Feb 1;2(2). Available from: http://perspectivesinmedicine.cshlp.org/content/2/2/a009399.abstract
19. Sulzer D, Edwards RH. The physiological role of α-synuclein and its relationship to Parkinson's Disease. J Neurochem [Internet]. 2019 Sep 1;150(5):475–86. Available from: https://doi.org/10.1111/jnc.14810
20. Becket G-H, Manuela P, Megumi M-T, Ling D, M. WA, H. NE, et al. αβγ-Synuclein triple knockout mice reveal age-dependent neuronal dysfunction. Proc Natl Acad Sci [Internet]. 2010 Nov 9;107(45):19573–8. Available from: https://doi.org/10.1073/pnas.1005005107
21. Kokhan VS, Afanasyeva MA, Van'kin GI. α-Synuclein knockout mice have cognitive impairments. Behav Brain Res. 2012;231(1):226–30.
22. Rousseaux MWC, Vázquez-Vélez GE, Al-Ramahi I, Jeong H-H, Bajić A, Revelli J-P, et al. A Druggable Genome Screen Identifies Modifiers of α-Synuclein Levels via a Tiered Cross-Species Validation Approach. J Neurosci [Internet]. 2018;38(43):9286. Available from: http://www.jneurosci.org/content/38/43/9286.abstract
23. Shu F, Lv S, Qin Y, Ma X, Wang X, Peng X, et al. Functional characterization of human PFTK1 as a cyclin-dependent kinase. Proc Natl Acad Sci U S A [Internet]. 2007/05/21.

2007 May 29;104(22):9248–53. Available from: https://pubmed.ncbi.nlm.nih.gov/17517622

24. Chen L, Wang Y, Jiang W, Ni R, Wang Y, Ni S. CDK14 involvement in proliferation migration and invasion of esophageal cancer. Ann Transl Med [Internet]. 2019 Nov;7(22):681. Available from: https://pubmed.ncbi.nlm.nih.gov/31930082
25. Zhou Y, Rideout WM, Bressel A, Yalavarthi S, Zi T, Potz D, et al. Spontaneous genomic alterations in a chimeric model of colorectal cancer enable metastasis and guide effective combinatorial therapy. PLoS One. 2014;9(8):1–13.
26. Ferguson FM, Doctor ZM, Ficarro SB, Browne CM, Marto JA, Johnson JL, et al. Discovery of Covalent CDK14 Inhibitors with Pan-TAIRE Family Specificity. Cell Chem Biol [Internet]. 2019;26(6):804-817.e12. Available from: http://www.sciencedirect.com/science/article/pii/S2451945619300704
27. Rodríguez González Y, Kamkar F, Jafar-nejad P, Wang S, Qu D, Sanchez Alvarez L, et al. PFTK1 kinase regulates axogenesis during development via RhoA activation. bioRxiv [Internet]. 2022 Jan 1;2022.01.11.475789. Available from: http://biorxiv.org/content/early/2022/03/10/2022.01.11.475789.abstract
28. Luk KC, Kehm V, Carroll J, Zhang B, O'Brien P, Trojanowski JQ, et al. Pathological α-Synuclein Transmission Initiates Parkinson-like Neurodegeneration in Nontransgenic Mice. Science (80- ) [Internet]. 2012;338(6109):949. Available from: http://science.sciencemag.org/content/338/6109/949.abstract
29. Mao X, Ou MT, Karuppagounder SS, Kam T-I, Yin X, Xiong Y, et al. Pathological α-synuclein transmission initiated by binding lymphocyte-activation gene 3. Science [Internet]. 2016 Sep 30;353(6307):aah3374. Available from: https://pubmed.ncbi.nlm.nih.gov/27708076
30. Kam T-I, Mao X, Park H, Chou S-C, Karuppagounder SS, Umanah GE, et al. Poly(ADP-ribose) drives pathologic α-synuclein neurodegeneration in Parkinson's disease. Science [Internet]. 2018 Nov 2;362(6414):eaat8407. Available from: https://pubmed.ncbi.nlm.nih.gov/30385548
31. Rockenstein E, Mallory M, Hashimoto M, Song D, Shults CW, Lang I, et al. Differential neuropathological alterations in transgenic mice expressing α-synuclein from the platelet-derived growth factor and Thy-1 promoters. J Neurosci Res. 2002 Jun;68(5):568–78.
32. Chesselet M-F, Richter F, Zhu C, Magen I, Watson MB, Subramaniam SR. A progressive mouse model of Parkinson's disease: the Thy1-aSyn ("Line 61") mice. Neurotherapeutics [Internet]. 2012;9(2):297–314. Available from: https://pubmed.ncbi.nlm.nih.gov/22350713
33. Matsuura K, Kabuto H, Makino H, Ogawa N. Pole test is a useful method for evaluating the mouse movement disorder caused by striatal dopamine depletion. J Neurosci Methods [Internet]. 1997;73(1):45–8. Available from: https://www.sciencedirect.com/science/article/pii/S016502709602211X
34. Sedelis M, Schwarting RKW, Huston JP. Behavioral phenotyping of the MPTP mouse model of Parkinson's disease. Behav Brain Res [Internet]. 2001;125(1):109–25. Available from: https://www.sciencedirect.com/science/article/pii/S0166432801003096
35. Dhungel N, Eleuteri S, Li L, Kramer NJ, Chartron JW, Spencer B, et al. Parkinson's Disease Genes VPS35 and EIF4G1 Interact Genetically and Converge on α-Synuclein. Neuron [Internet]. 2015;85(1):76–87. Available from: https://www.sciencedirect.com/science/article/pii/S0896627314010812

36. Rousseaux MWC, de Haro M, Lasagna-Reeves CA, De Maio A, Park J, Jafar-Nejad P, et al. TRIM28 regulates the nuclear accumulation and toxicity of both alpha-synuclein and tau. Ackerman SL, editor. Elife [Internet]. 2016;5:e19809. Available from: https://doi.org/10.7554/eLife.19809
37. Rockenstein E, Clarke J, Viel C, Panarello N, Treleaven CM, Kim C, et al. Glucocerebrosidase modulates cognitive and motor activities in murine models of Parkinson's disease. Hum Mol Genet [Internet]. 2016 Jul 1;25(13):2645–60. Available from: https://doi.org/10.1093/hmg/ddw124
38. Soldner F, Laganière J, Cheng AW, Hockemeyer D, Gao Q, Alagappan R, et al. Generation of Isogenic Pluripotent Stem Cells Differing Exclusively at Two Early Onset Parkinson Point Mutations. Cell [Internet]. 2011;146(2):318–31. Available from: https://www.sciencedirect.com/science/article/pii/S0092867411006611
39. Bhullar KS, Lagarón NO, McGowan EM, Parmar I, Jha A, Hubbard BP, et al. Kinase-targeted cancer therapies: progress, challenges and future directions. Mol Cancer [Internet]. 2018 Feb 19;17(1):48. Available from: https://pubmed.ncbi.nlm.nih.gov/29455673
40. Gouda NA, Elkamhawy A, Cho J. Emerging Therapeutic Strategies for Parkinson’s Disease and Future Prospects: A 2021 Update. Vol. 10, Biomedicines . 2022.
41. Tomlinson JJ, Shutinoski B, Dong L, Meng F, Elleithy D, Lengacher NA, et al. Holocranohistochemistry enables the visualization of α-synuclein expression in the murine olfactory system and discovery of its systemic anti-microbial effects. J Neural Transm [Internet]. 2017;124(6):721–38. Available from: https://doi.org/10.1007/s00702-017-1726-7
42. L. BE, Aaron M, D. SK, S. BK, Mastooreh C, E. MT, et al. Alpha-Synuclein Expression Restricts RNA Viral Infections in the Brain. J Virol [Internet]. 2022 May 2;90(6):2767–82. Available from: https://doi.org/10.1128/JVI.02949-15
43. Allen Reish HE, Standaert DG. Role of α-synuclein in inducing innate and adaptive immunity in Parkinson disease. J Parkinsons Dis [Internet]. 2015;5(1):1–19. Available from: https://pubmed.ncbi.nlm.nih.gov/25588354
44. Rousseaux MWC, Revelli J-P, Vázquez-Vélez GE, Kim J-Y, Craigen E, Gonzales K, et al. Depleting Trim28 in adult mice is well tolerated and reduces levels of α-synuclein and tau. Ackerman SL, editor. Elife [Internet]. 2018;7:e36768. Available from: https://doi.org/10.7554/eLife.36768
45. Karczewski KJ, Francioli LC, Tiao G, Cummings BB, Alföldi J, Wang Q, et al. The mutational constraint spectrum quantified from variation in 141,456 humans. Nature [Internet]. 2020;581(7809):434–43. Available from: https://doi.org/10.1038/s41586-020-2308-7
46. Volpicelli-Daley LA, Luk KC, Patel TP, Tanik SA, Riddle DM, Stieber A, et al. Exogenous α-synuclein fibrils induce Lewy body pathology leading to synaptic dysfunction and neuron death. Neuron [Internet]. 2011 Oct 6;72(1):57–71. Available from: https://pubmed.ncbi.nlm.nih.gov/21982369
47. Polinski NK, Volpicelli-Daley LA, Sortwell CE, Luk KC, Cremades N, Gottler LM, et al. Best Practices for Generating and Using Alpha-Synuclein Pre-Formed Fibrils to Model Parkinson's Disease in Rodents. J Parkinsons Dis [Internet]. 2018;8(2):303–22. Available from: https://pubmed.ncbi.nlm.nih.gov/29400668

48. Deacon R. Assessing burrowing, nest construction, and hoarding in mice. J Vis Exp [Internet]. 2012 Jan 5;(59):e2607–e2607. Available from: https://pubmed.ncbi.nlm.nih.gov/22258546
49. Ryan SD, Dolatabadi N, Chan SF, Zhang X, Akhtar MW, Parker J, et al. Isogenic Human iPSC Parkinson's Model Shows Nitrosative Stress-Induced Dysfunction in MEF2-PGC1α Transcription. Cell [Internet]. 2013;155(6):1351–64. Available from: http://www.sciencedirect.com/science/article/pii/S0092867413014220
50. Kriks S, Shim J-W, Piao J, Ganat YM, Wakeman DR, Xie Z, et al. Dopamine neurons derived from human ES cells efficiently engraft in animal models of Parkinson's disease. Nature [Internet]. 2011;480(7378):547–51. Available from: https://doi.org/10.1038/nature10648
51. Bojan S, Mansoureh H, E. HI, Michaela L, Juliana R, Nathalie L, et al. Lrrk2 alleles modulate inflammation during microbial infection of mice in a sex-dependent manner. Sci Transl Med [Internet]. 2019 Sep 25;11(511):eaas9292. Available from: https://doi.org/10.1126/scitranslmed.aas9292
52. Volpicelli-Daley LA, Luk KC, Lee VM-Y. Addition of exogenous α-synuclein preformed fibrils to primary neuronal cultures to seed recruitment of endogenous α-synuclein to Lewy body and Lewy neurite–like aggregates. Nat Protoc [Internet]. 2014;9(9):2135–46. Available from: https://doi.org/10.1038/nprot.2014.143

**Acknowledgments:**

The authors thank Drs. Robert Rissman (UCSD), Eliezer Masliah (UCSD/NIA) and David Park (University of Calgary) for sharing the mutant mice used in this study. We thank Dr. G. Vázquez-Vélez (Washington University) for his critical appraisal of the manuscript. The authors also thank the following Core facilities from the University of Ottawa and the Ottawa Hospital Research Institute for use of their facility, equipment, and expertise: Animal Behaviour and Physiology Core, Cell Biology and Imaging Acquisition Core, StemCore Laboratories and Louise Pelletier Histology Core. Schemes were generated using biorender (https://biorender.com/).

**Funding:**

Parkinson's Foundation-APDA Summer Student Fellowship PF-APDA-SFW-1919, Parkinson Research Consortium (PRC) Summer Studentship, University of Ottawa Faculty of Medicine, Office of Francophones Affairs Scholarship. (JLAP)
Parkinson Research Consortium (PRC) Larry Haffner Fellowship, Parkinson Canada Basic Research Fellowship BRF-2021-0000000048. (KMR)
Parkinson's Research Consortium (PRC) Bonnie and Don Poole Fellowship, Ontario Graduate Scholarship, Queen Elizabeth II Scholarship. (HMG)

742 Canadian Institutes of Health Research (FRN-153188). (WLS)
743 Vanier Canada. (MGS)
744 Parkinson's Society of Southwestern Ontario (PSSO). (BBD)
745 Canadian Institutes of Health Research (FRN-159443). (SDR)
746 Parkinson's Foundation Stanley Fahn Junior Faculty Award (PF-JFA-1762), Canadian
747 Institutes of Health Research (PJT-169097), the Parkinson Canada New Investigator
748 Award (2018-00016), Aligning Science Across Parkinson's (ASAP-020625) through the
749 Michael J. Fox Foundation for Parkinson's Research (MJFF). (MWCR)

750

751 **Author contributions:**

752 Conceptualization: JLAP, KMR, MWCR
753 Methodology: JLAP, KMR, MS, BBD, EL, BN, NAL, HMG, AB, MGS, BBD, SMC,
754 MWCR
755 Investigation: JLAP, KMR, MS, BBD, HMG, SMC, MWCR
756 Supervision: WLS, MGS, SDR, MWCR
757 Writing – original draft: JLAP, KMR, MWCR
758 Writing – review & editing: JLAP, KMR, JJT, MGS, WLS, PB, SDR, MWCR
759 Resources: AJ, PB

760

761 **Competing interests:**

762 The authors declare that they have no conflict of interest.

763

764 **Data and materials availability:**

765 All data of this study are in the main text or in the Supplementary Materials. Cdk14$^{+/-}$ and Cdk14$^{-}$
766 $^{/-}$ mice were obtained from David Park from the University of Calgary and are on an F14
767 C57BL/6N background. mThy1-SNCA "line 61" (*α-Syn TG*) mice were obtained from Robert
768 Rissman from the University of California, San Diego. Mouse α-Syn PFF preparations were
769 provided by Patrik Brundin, Van Andel Institute, Grand Rapids. Any other materials are
770 commercially available.

771

772

773 **Figures**

774 **Figure 1. Loss of Cdk14 ameliorates motor impairment and α-Syn pathology in PFF-injected**
775 **mice.** (A) Mouse α-Syn PFFs were injected unilaterally to the striatum by stereotactic injection in
776 6-month-old mice. (B) Loss of forelimb grip strength at 6 months post α-Syn PFF-treatment in
777 WT mice, but not in *Cdk14*$^{+/-}$- or *Cdk14*$^{-/-}$-mice. Two-way ANOVA, Bonferroni *post hoc,* n: 9-10.
778 (C) α-Syn PFF-injection increased the load of pS129 α-Syn-positive cells (depicted without and
779 with hematoxylin counterstaining, 50 µm scale bars) in the injected hemisphere (ipsilateral, IL).
780 Densities of pS129 α-Syn-positive cells are depicted in heat maps as hues of red at 3 rostrocaudal
781 levels (relative to bregma: +0.98 mm, +0.26 mm, and -1.34 mm) with dark shades of red
782 correlating to high cell densities. Amounts of pS129 α-Syn-positive cells in all brain regions
783 (averaged) and the somatomotor cortex at +0.26 mm relative to bregma of PFF-injected *Cdk14*$^{+/-}$
784 - and *Cdk14*$^{-/-}$- mice were lower relative to their wildtype (WT) counterparts. Two-way ANOVA,
785 Bonferroni *post hoc* comparisons*,* n: 3-6.

786

787 **Figure 2. Cdk14 modulates PD-like behavior and regulates α-Syn levels in mice**
788 **overexpressing human α-Syn.** (A) Breeding strategy to obtain *α-Syn TG; Cdk14*$^{+/-}$-mice. (B)
789 Elevated turn latencies during pole test experiments were observed in *α-Syn TG*-, but not in *α-Syn*
790 *TG; Cdk14*$^{+/-}$-mice. Two-way ANOVA, Bonferroni *post hoc* comparisons. (C) *α-Syn TG*- and *α-*
791 *Syn TG; Cdk14*$^{+/-}$-mice display similar hyperactive locomotion in beam break experiments when
792 compared to WT mice. Repeated measures two-way ANOVA, Bonferroni *post hoc* comparisons.
793 (D) Nest building quality is similarly reduced in 3-monht-old *α-Syn TG*- and *α-Syn TG; Cdk14*$^{+/-}$-
794 mice. Two-way ANOVA, Bonferroni *post hoc* comparisons, n: 15-19. (E) Immunoblots depicting
795 the levels of pS129 α-Syn, total α-Syn, Cdk14, and GAPDH in the NETN buffer-soluble and -

796 insoluble protein fraction of mouse hemibrains. Brains of *Cdk14*$^{+/-}$-mice contain less total α-Syn
797 than brains of WT mice. Partial ablation of *Cdk14* in *α-Syn TG* results in elevated levels of pS129
798 α-Syn in the soluble fraction and decreased total α-Syn levels in the insoluble fraction. Unpaired
799 student's *t* tests, n:5-7.

800

801 **Figure 3. Genetic reduction of Cdk14 prevents neuron loss in *α-Syn TG* mice and mildens α-**
802 **Syn pathology in human neurons.** Immunofluorescence staining for NeuN in the Ca3 region of
803 the hippocampus (A, 200 µm scale bar) and layer V of the cortex (B, 100 µm scale bar) visualize
804 reduced neuronal densities in *α-Syn TG* mice which is not observed in *α-Syn TG; Cdk14*$^{+/-}$-mice.
805 Two-way ANOVA, Bonferroni *post hoc* comparisons, n=5. (C) Immunoblots illustrating elevated
806 amounts of pS129 α-Syn in hiPSC-derived *SNCA* A53T human neurons (in comparison to isogenic
807 corrected neurons [Corr]) which is reduced by CRISPR/Cas9-mediated knockdown of *CDK14*
808 (targeted against *CDK14* exon 3 (E3) and 8 (E8)). One-way ANOVA, Tukey *post hoc*
809 comparisons, n=3-4.

810

811 **Figure 4. Pharmacological inhibition of CDK14 reduces α-Syn protein burdens in human**
812 **and rodent neurons.** (A) Application of 500 nM of the CDK14 inhibitor FMF-04-159-2 for 18
813 hours to HEK293T cells decreases CDK14 and α-Syn levels, as shown by immunoblots. Unpaired
814 student's *t* tests, n=6. (B) Dose-dependent reduction of α-Syn in hESC-derived human neurons is
815 detected by ELISA quantification after 72 hours of CDK14 inhibitor treatment. One-way ANOVA,
816 Bonferroni *post hoc* comparisons, n=3. (C) Human α-Syn PFFs applied to rat cortical neurons
817 increase the amount of α-Syn, as shown by immunoblots, which was reduced by the application of

818 100 nM of the CDK14 inhibitor for 5 days. Repeated measures one-way ANOVA, followed by

819 Holm-Šídák *post hoc* comparisons, n=3.

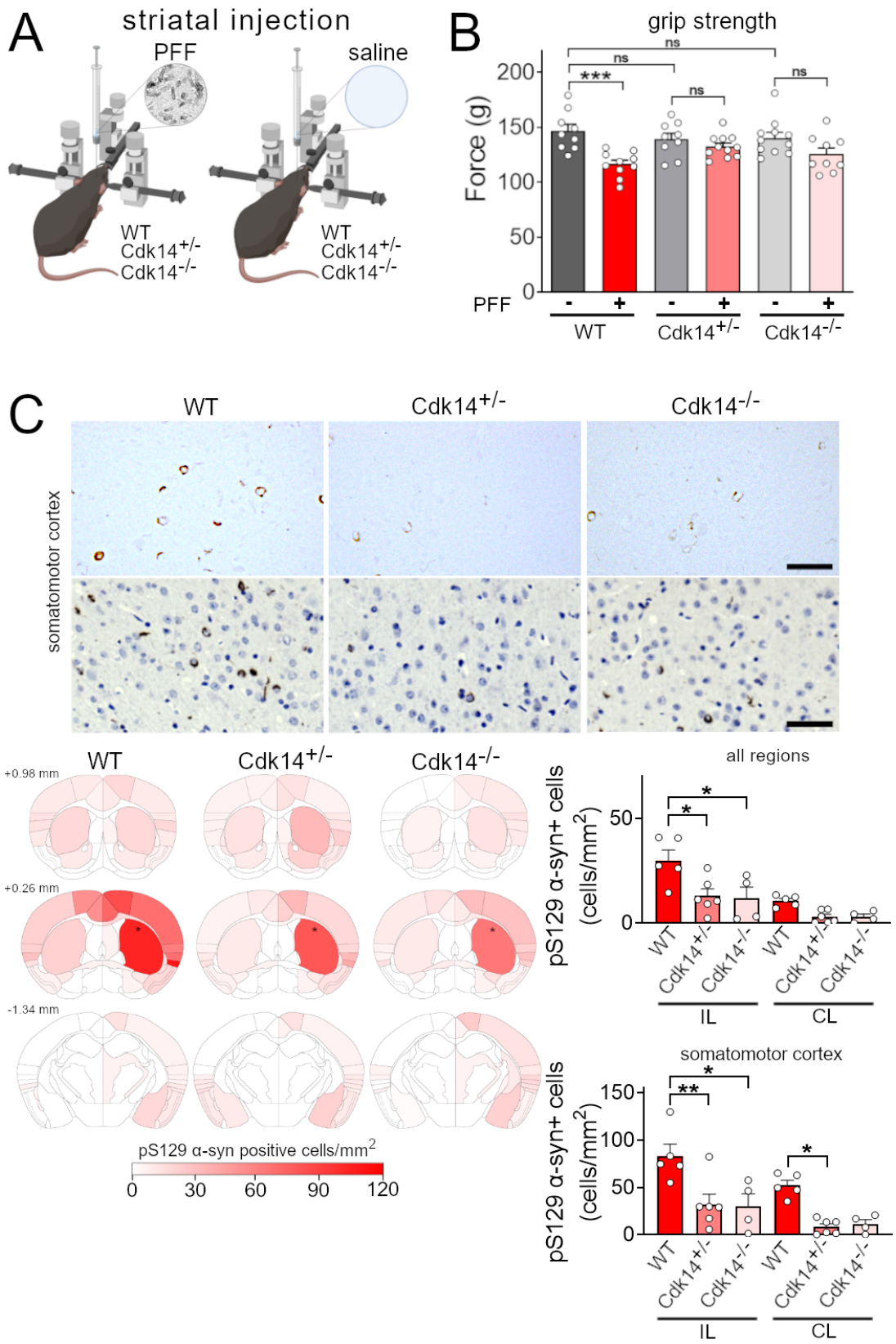
A
striatal injection
PFF
saline
WT
Cdk14+/-
Cdk14-/-
B
grip strength
Force (g)
ns
***
PFF
C
WT
Cdk14+/-
Cdk14-/-
somatomotor cortex
+0.98 mm
+0.26 mm
-1.34 mm
pS129 α-syn positive cells/mm2
all regions
somatomotor cortex
pS129 α-syn+ cells (cells/mm2)
IL
CL

**Fig. 1**

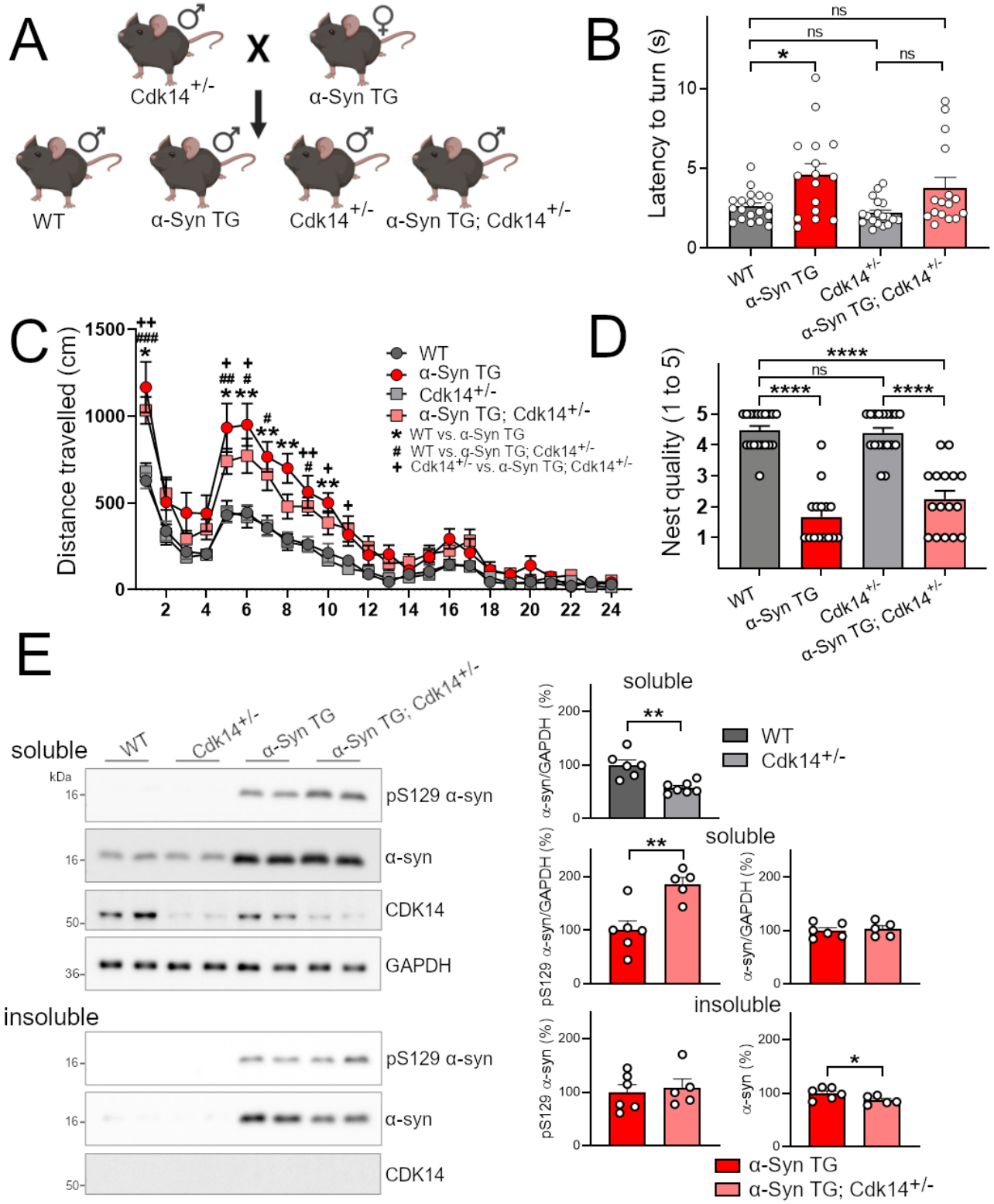
A
Cdk14+/-
x
α-Syn TG
WT
α-Syn TG
Cdk14+/-
α-Syn TG; Cdk14+/-
B
Latency to turn (s)
ns
ns
*
ns
WT
α-Syn TG
Cdk14+/-
α-Syn TG; Cdk14+/-
C
Distance travelled (cm)
WT
α-Syn TG
Cdk14+/-
α-Syn TG; Cdk14+/-
* WT vs. α-Syn TG
# WT vs. α-Syn TG; Cdk14+/-
+ Cdk14+/- vs. α-Syn TG; Cdk14+/-
D
Nest quality (1 to 5)
****
ns
****
****
WT
α-Syn TG
Cdk14+/-
α-Syn TG; Cdk14+/-
E
soluble
WT
Cdk14+/-
α-Syn TG
α-Syn TG; Cdk14+/-
kDa
pS129 α-syn
α-syn
CDK14
GAPDH
insoluble
pS129 α-syn
α-syn
CDK14
α-syn/GAPDH (%)
pS129 α-syn/GAPDH (%)
pS129 α-syn (%)
α-syn (%)
WT
Cdk14+/-
α-Syn TG
α-Syn TG; Cdk14+/-

**Fig. 2**

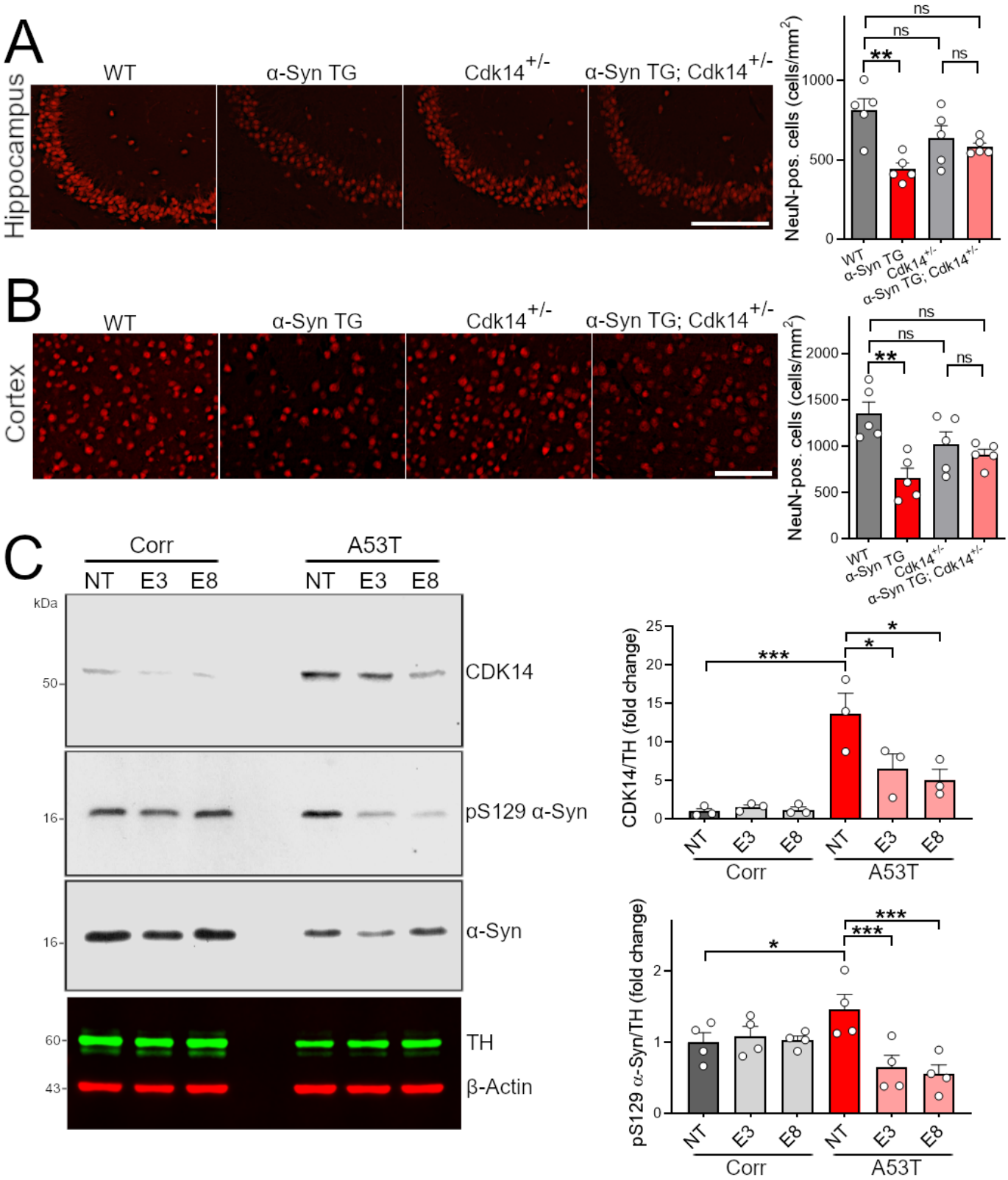
A
Hippocampus
WT
α-Syn TG
Cdk14+/-
α-Syn TG; Cdk14+/-
NeuN-pos. cells (cells/mm2)
ns
ns
ns
**
B
Cortex
C
Corr
A53T
NT
E3
E8
kDa
CDK14
pS129 α-Syn
α-Syn
TH
β-Actin
CDK14/TH (fold change)
pS129 α-Syn/TH (fold change)
***
*

824

825 **Fig. 3**

826

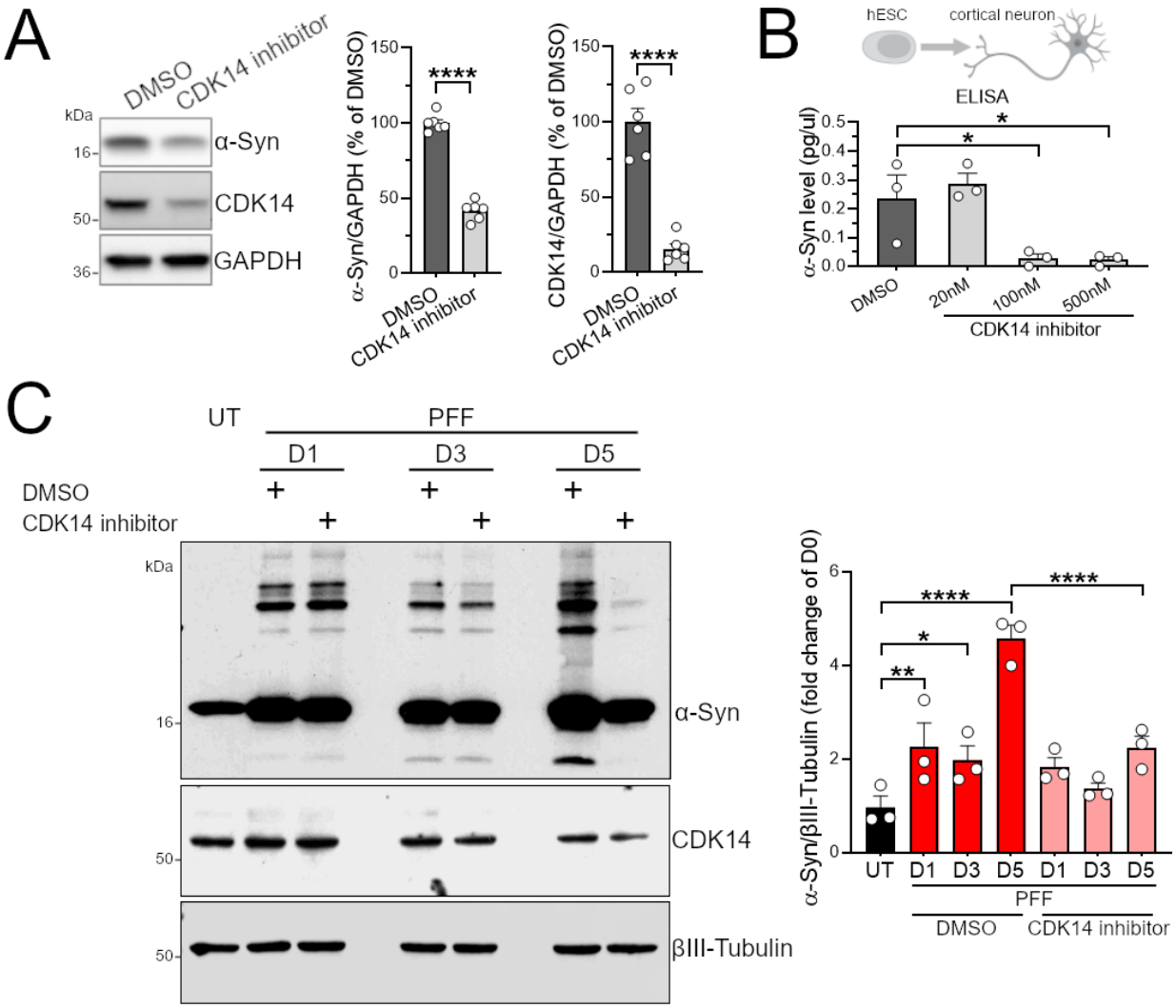


827

828 **Fig. 4**

829

830 **Supplementary Materials**

831

832 **Figure S1. Cdk14 protein levels in mouse organs and mouse α-Syn PFF characterization.** (A)
833 Immunoblots depicting Cdk14 protein from different organs of *Cdk14*$^{-/-}$- and WT-mice. (B)
834 Transmission electron micrograph (500 nm scale) illustrating mouse α-Syn PFFs used for
835 intrastriatal injections and corresponding α-Syn PFF length analysis.

836

837 **Figure S2. Behavioral profile and dopaminergic striatal fiber density of PFF injected *Cdk14*$^{-}$**
838 **$^{/-}$-mice.** (A) 12-month-old *Cdk14*$^{+/-}$ and *Cdk14*$^{-/-}$- mice do not display altered behavior in the
839 nesting, tail suspension, elevated plus maze, Y maze, open field, hanging wire, pole (two-way
840 ANOVA, Bonferroni *post hoc* comparisons) and rotarod test (repeated measures two-way
841 ANOVA, Bonferroni *post hoc* comparisons, n:9-10). PFF treatment does not result in significant
842 changes of behavior at 6 months post injection. (B) PFF injection does not change striatal tyrosine
843 hydroxylase (TH)-positive fiber density in the ipsilateral side (IL) in comparison to the non-
844 injected, contralateral side (CL) at bregma 0.26 mm (200 µm scale). Two-way ANOVA,
845 Bonferroni *post hoc* comparisons, n: 3-7.

846

847 **Figure S3. Histopathology in *α-Syn TG; Cdk14*$^{+/-}$-mice and α-Syn protein levels in rat**
848 **primary neurons.** (A) Cortical pS129 α-Syn signal intensities do not differ between *α-Syn TG*-
849 and *α-Syn TG; Cdk14*$^{+/-}$-mice (200 µm scale). Two-way ANOVA, Bonferroni *post hoc*
850 comparisons, n=4-5. (B) *α-Syn TG*- and *α-Syn TG; Cdk14*$^{+/-}$-mice display similar degrees of
851 astrogliosis in the hippocampus, visualized by GFAP staining (200 µm scale). Two-way ANOVA,
852 Bonferroni *post hoc* comparisons, n=5. (C) For protein degradation experiments, HEK293T cells

853 were treated with 500 nM FMF-04-159-2, 1 μM MG-132 and 200 nM Bafilomycin A1 for 18
854 hours. Activity of the ubiquitin proteasome system and autophagy is visualized with immunoblots
855 by Ubiquitin and LC3B, respectively. Two-way ANOVA, Bonferroni *post hoc* comparisons, n=3.
856 Application of 500 nM of FMF-04-159-2 for 18 hours to HEK293T cells decreases *SNCA*
857 transcript levels, quantified by qPCR. Unpaired student's *t* tests, n=6. (D) Rat cortical neurons
858 treated with α-Syn monomers do not present with elevated amounts of α-Syn monomers. Repeated
859 measures one-way ANOVA, followed by Holm-Šídák *post hoc* comparisons, n=3.
860

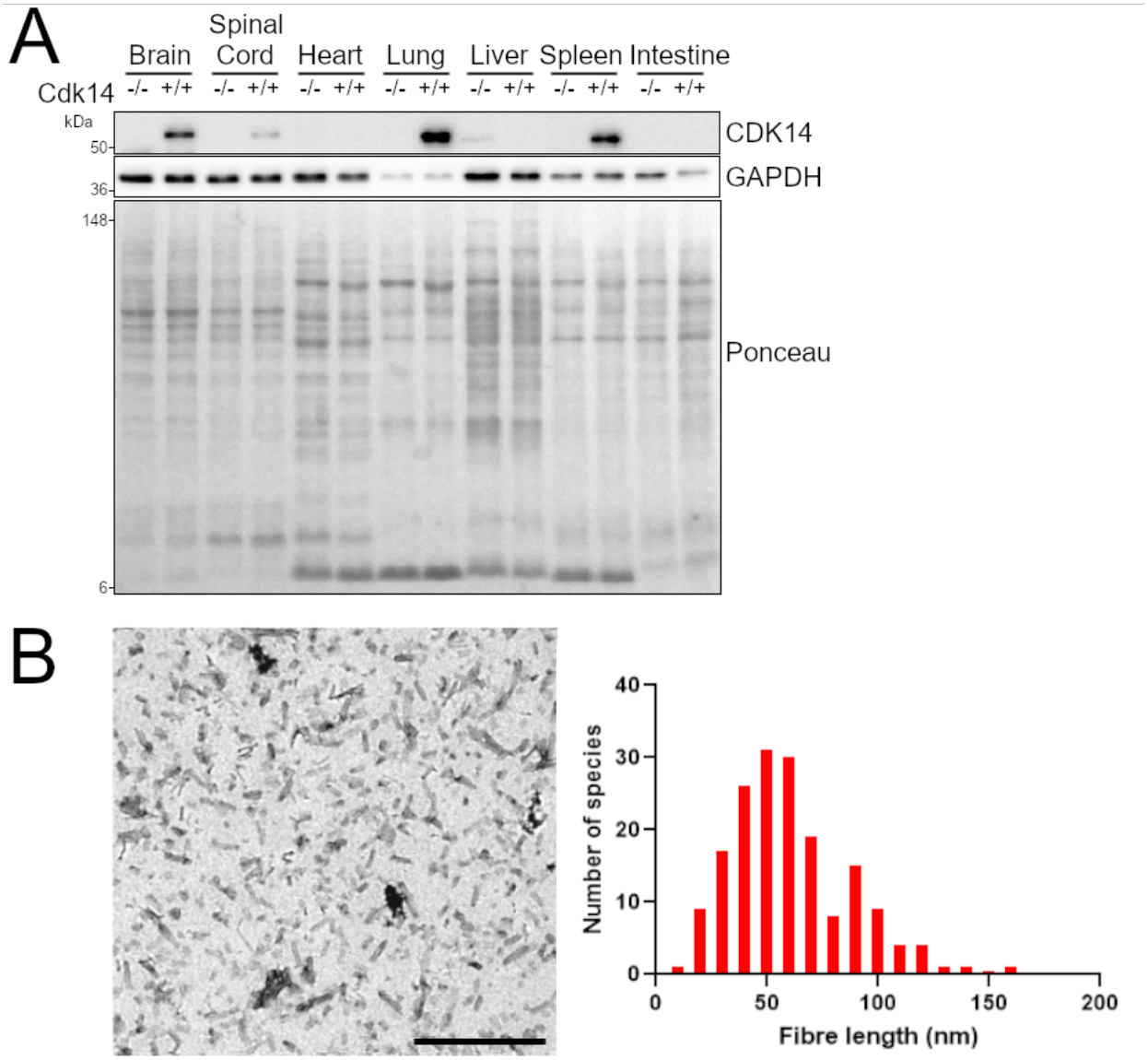
A
Brain
Spinal Cord
Heart
Lung
Liver
Spleen
Intestine
Cdk14
-/- +/+ -/- +/+ -/- +/+ -/- +/+ -/- +/+ -/- +/+ -/- +/+
kDa
50
36
148
6
CDK14
GAPDH
Ponceau
B
Number of species
Fibre length (nm)
0
10
20
30
40
0
50
100
150
200

**Fig. S1.**

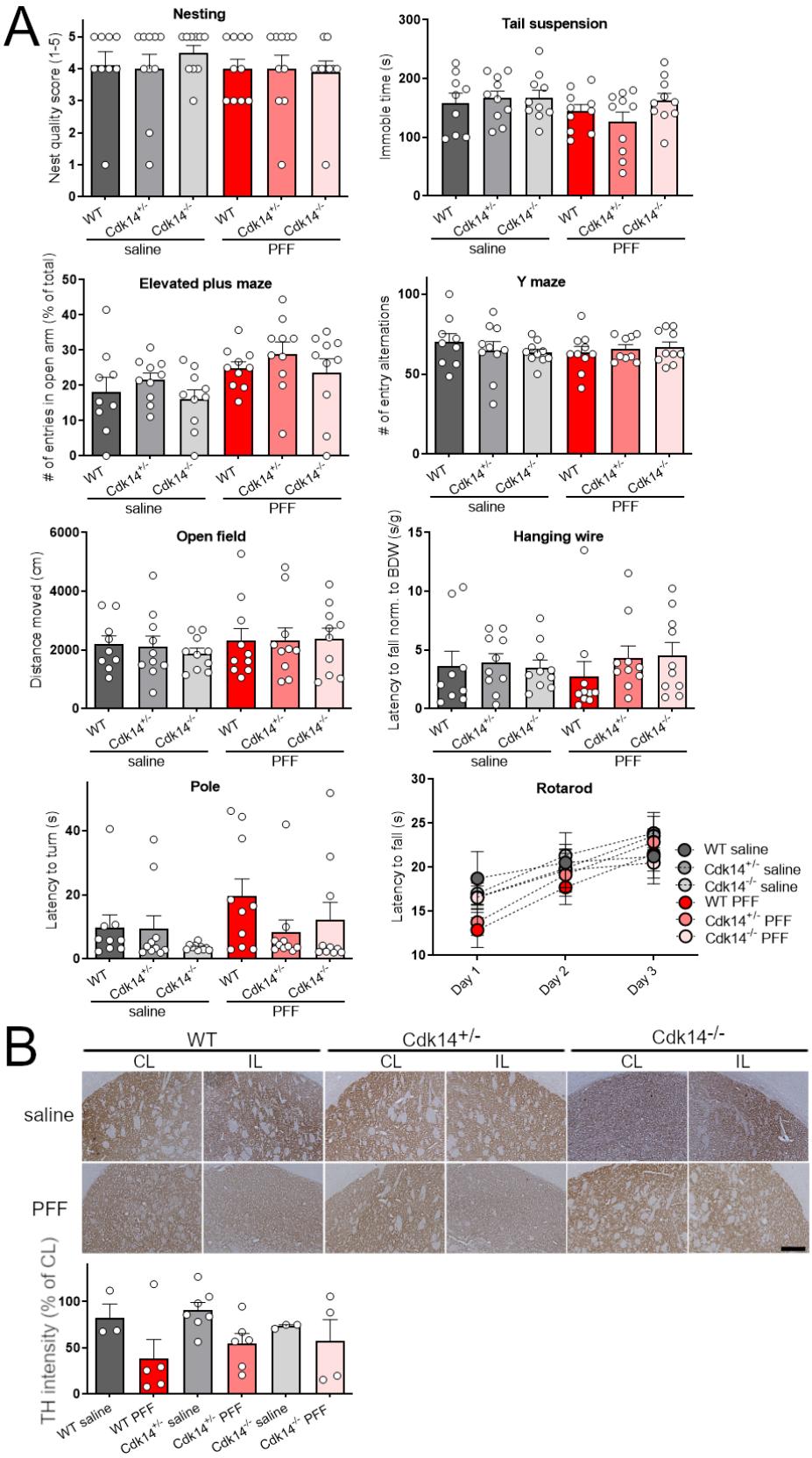
A
Nesting
Nest quality score (1-5)
Tail suspension
Immobile time (s)
Elevated plus maze
# of entries in open arm (% of total)
Y maze
# of entry alternations
Open field
Distance moved (cm)
Hanging wire
Latency to fall norm. to BDW (s/g)
Pole
Latency to turn (s)
Rotarod
Latency to fall (s)
Day 1
Day 2
Day 3
WT saline
Cdk14+/- saline
Cdk14-/- saline
WT PFF
Cdk14+/- PFF
Cdk14-/- PFF
WT
Cdk14+/-
Cdk14-/-
saline
PFF
B
WT
Cdk14+/-
Cdk14-/-
CL
IL
saline
PFF
TH intensity (% of CL)
WT saline
WT PFF
Cdk14+/- saline
Cdk14+/- PFF
Cdk14-/- saline
Cdk14-/- PFF

**Fig. S2**

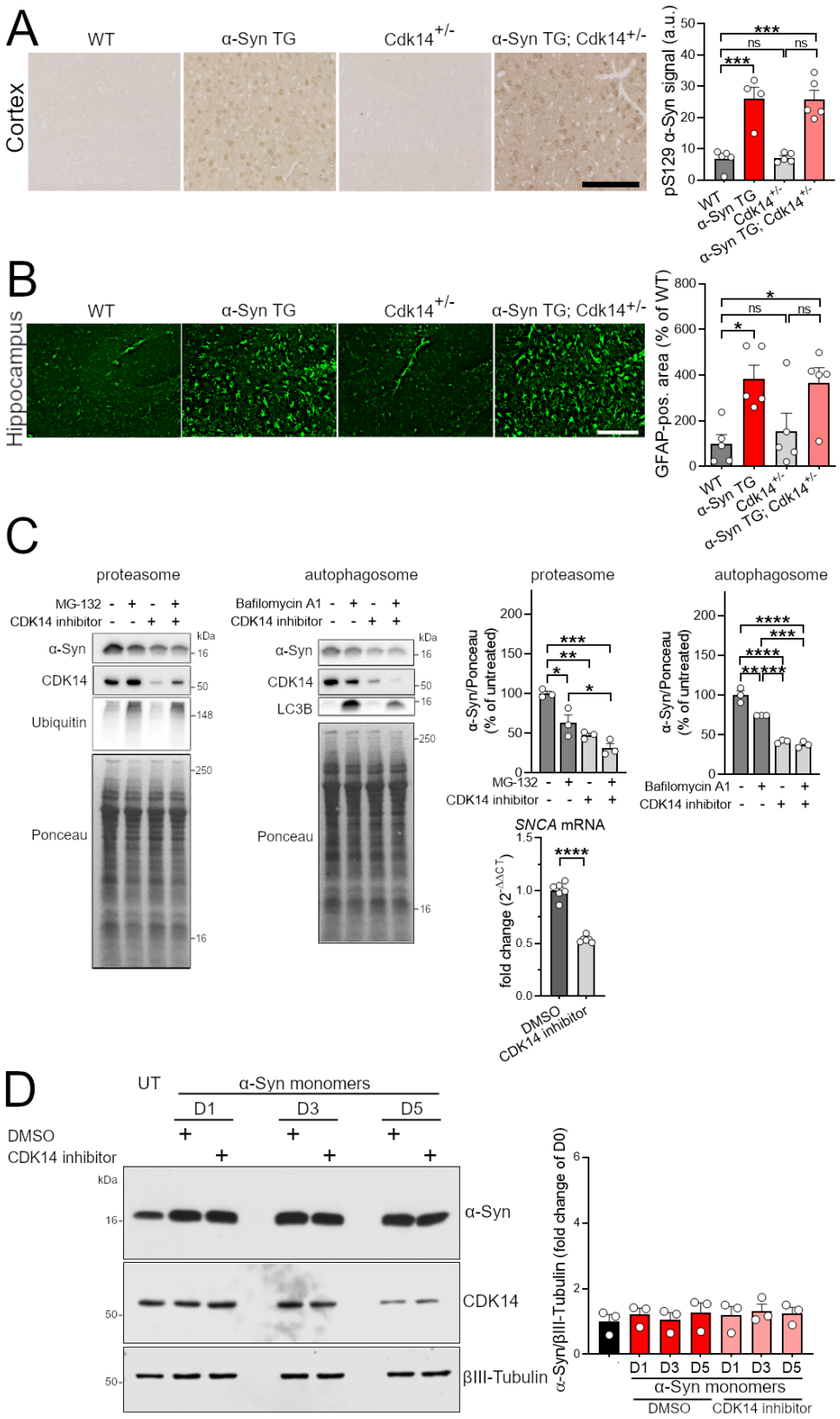
A
WT
α-Syn TG
Cdk14+/-
α-Syn TG; Cdk14+/-
Cortex
pS129 α-Syn signal (a.u.)
B
Hippocampus
GFAP-pos. area (% of WT)
C
proteasome
autophagosome
MG-132
Bafilomycin A1
CDK14 inhibitor
α-Syn
CDK14
Ubiquitin
LC3B
Ponceau
kDa
α-Syn/Ponceau (% of untreated)
SNCA mRNA
fold change (2-ΔΔCT)
DMSO
CDK14 inhibitor
D
UT
α-Syn monomers
D1
D3
D5
βIII-Tubulin
α-Syn/βIII-Tubulin (fold change of D0)

**Fig. S3**